Department of the Navy
Bureau of Ships
Contract Nonr-220(12)

EXPERIMENTS ON CIRCULAR ARC AND FLAT PLATE HYDROFOILS IN NONCAVITATING AND FULL CAVITY FLOWS

Blaine R. Parkin

This research was carried out under the Bureau of Ships
Fundamental Hydromechanics Research Program
Project NS 715-102, David Taylor Model Basin

Hydrodynamics Laboratory
California Institute of Technology
Pasadena, California

Report No. 47-6
February, 1956

Approved:
M.S. Plesset

TABLE OF CONTENTS

ABSTRACT

An investigation in the High Speed Water Tunnel of the two-dimensional hydrodynamic characteristics of sharp-edged hydrofoils is described. The lift, drag, and pitching moment were measured in cavitating and noncavitating flows for flat plate and circular arc profiles. The theory of Wu for the forces on sharp-edged profiles in full cavity flow and the experimental results showed good agreement over a wide range of attack angles.

INTRODUCTION

The primary advantage to be gained from hydrofoil boats is the possibility of attaining very high operating speeds without inordinately high power requirements. However, the fullest exploitation of this important advantage may make the occurrence of cavitation on the hydrofoil system unavoidable with a resulting increase in drag and a decrease in lift. For some applications where very high speeds are essential, it may be possible to relax the requirement for a high lift coefficient and, if the cavitating hydrofoils operate in a stable manner, the onset of cavitation need pose no insurmountable problem. In fact it may be desirable to operate the hydrofoils over the greatest possible speed range in the fully cavitating regime in order to take fullest advantage of this stable flow configuration. Thus, we are lead naturally to profiles with sharp leading and trailing edges because the very low minimum pressures provided by their sharp edges make such profiles cavitate at relatively low speeds. Moreover, for full cavity flows the cavity springs from the sharp edges, so for a large range of attack angles the

geometry of the flow past the hydrofoil remains essentially the same, thereby assuring steady hydrofoil operation. On the other hand, there are situations in which the onset of full cavity flow completely changes the flow geometry so that the forces on the hydrofoil suffer drastic changes as the full cavity develops. The nature of such force variations and the range of flow geometries for which they occur should be of considerable interest for the application of sharp-edged profiles to design situations.

In view of the fact that the full cavity generally springs from the sharp leading and trailing edges, the two-dimensional cavity flow past such sharp-edged profiles of simple geometry has considerable theoretical interest. These fixed separation points enable free streamline theory to be applied to a cavity flow for which the separation points are known in advance. Such a theory of forces on fully cavitating profiles has been developed by T. Y. Wu.[1] It is of interest to submit this theory, which makes no linearizing approximations, to experimental verification.

The present report includes a presentation of the two-dimensional force and moment characteristics which were obtained in High Speed Water Tunnel[2] experiments. These data are presented for sharp-edged hydrofoils of flat plate, and concave circular arc profiles for both cavitating and noncavitating flow. Those forces which were measured in the fully cavitating flow regime are compared with Wu's exact theory.

EXPERIMENTAL PROCEDURES

The methods of measurement and of data reduction will be described in this section. Brief descriptions of the experimental equipment used in the experiments are also given.

The present experiments, which were made to determine the two-dimensional forces on flat plate and circular arc profiles in full cavity flow, required that a two-dimensional channel be installed in the High Speed Water Tunnel working section. When this modification to the High

Speed Water Tunnel working section is made, the test section is changed from a round channel 14 inches in diameter into a nearly rectangular section which is 14 inches high and 3 inches wide. This modification is accomplished by simply bolting appropriate plates and castings into the existing round test section as shown by Figs. 1 and 2. A detailed flow calibration of this two-dimensional section, which has been carried out by Kermeen[3] showed the flow to be very uniform except near the walls where boundary layer effects are important. The boundary layer thickness on the vertical walls in the region spanned by the two-dimensional hydrofoil models was found to be about 3/16 inch.

A three-view schematic drawing which shows the two-dimensional working section, force balance, and the position of the hydrofoil is given in Fig. 3. The horizontal hydrofoil orientation was chosen in order to eliminate hydrostatic pressure effects on the spanwise distribution of cavitation. It has been found that with this precaution, the resulting flows are essentially two-dimensional under both cavitating and noncavitating conditions.

The profile shapes chosen for the experiments are shown to scale in Fig. 4. For strength, the flat plate profile is actually the lower surface of a narrow wedge of 10 degree-apex angle, and the circular arc model is of circular contour on only one face. Thus, for full cavity flows these two models allowed tests to be made for three different shapes; a flat plate, a concave circular arc and a bent plate. This last shape is obtained by running the circular arc model upside down so that the concave section is inside the cavity and the polygonal section is exposed to the liquid flow. The attack angles and cavitation conditions for which this last configuration could be tested were limited by the cavitation which occurred at the hump between the two flat surfaces. In the range of lower attack angles, the first segment in front of the hump is still wetted, while a full cavity develops over the rear segment. Data for this case had already been taken with the wedge.

Figure 5 shows the circular arc model attached to the mounting disk for installation of the model in the test section. Both models

were attached to mounting disks as shown, and then the disk was attached to the force balance spindle.[4] The flat portion of the disk was fitted to the spindle so that it was flush with the working section wall. The gap between the mounting disk and the over-sized hole in the wall was made as small as possible in order to reduce extraneous flows over the profiles. However, under some severe profile load conditions, spindle deflections allowed the mounting disk to bear against the side of the hole in the channel wall and thus prohibit the recording of valid force data. For those instances where it was necessary to obtain force data for such severe flow configurations, the tunnel velocity was lowered enough to reduce the spindle deflections to an acceptable amount. In the course of these experiments, a heavier spindle was installed to minimize these deflections.

Most of the force data were taken with the tunnel speed set for 30 or 25 fps. For each test run, lift, drag, and pitching moment data were taken at a constant velocity and at a constant attack angle. The forces were measured from noncavitating to full cavity flow conditions by varying the working section static pressure. This procedure was repeated for all the attack angles investigated. The forces and moments measured by the balance are read out on automatic beam balances. These readings were recorded photographically by means of a microfilm camera which was mounted over the gauge console as shown in Fig. 6. In the present experiments, only a few check runs were made to evaluate the experimental scatter, because it had already been found[3] that the present balance generally gives force and moment data which are reproducable within two or three per cent.

The force and moment data were corrected for force gauge readings at zero load, for the slight influence of working section static pressures on the balance readings, and for viscous drag on the hydrofoil mounting disk. None of these data were corrected for blockage or other wall effects. The data were reduced to coefficient form by means of the formulas

$$C_L = \frac{\text{Lift}}{\frac{1}{2}\rho V^2 A}, \qquad C_D = \frac{\text{Drag}}{\frac{1}{2}\rho V^2 A}, \qquad \text{and} \qquad C_M = \frac{\text{Moment}}{\frac{1}{2}\rho V^2 Ac}.$$

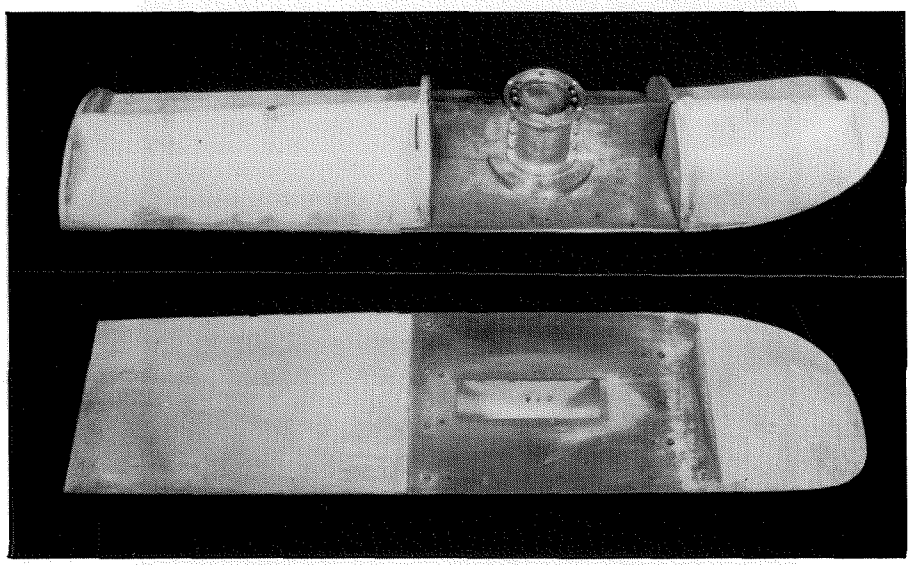

Fig. 1 - Fairing plates for converting the High Speed Water Tunnel test section into a two-dimensional channel.

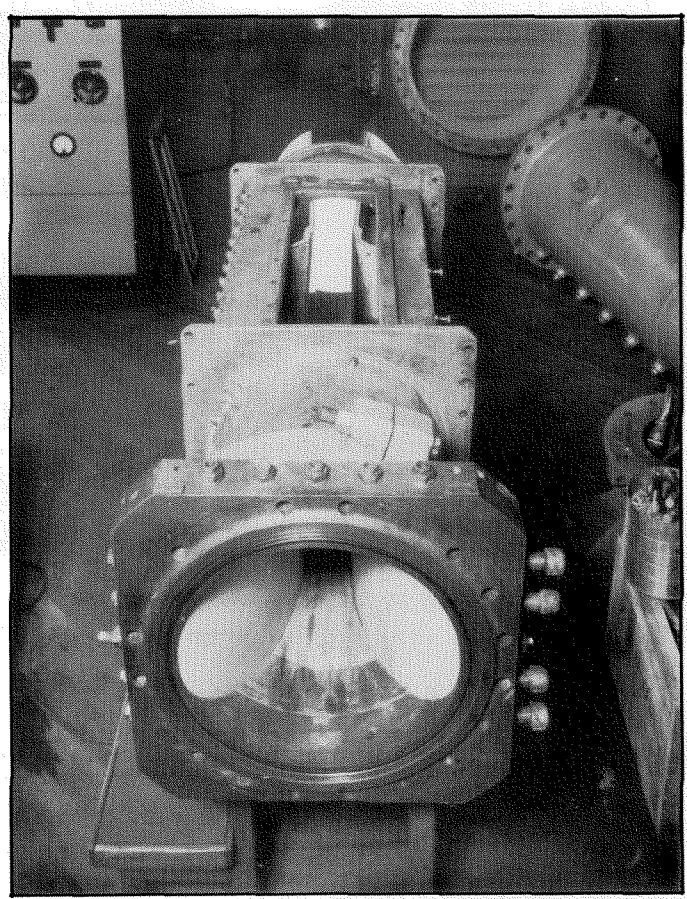

Fig. 2 - Fairing plates installed in the High Speed Water Tunnel test section.

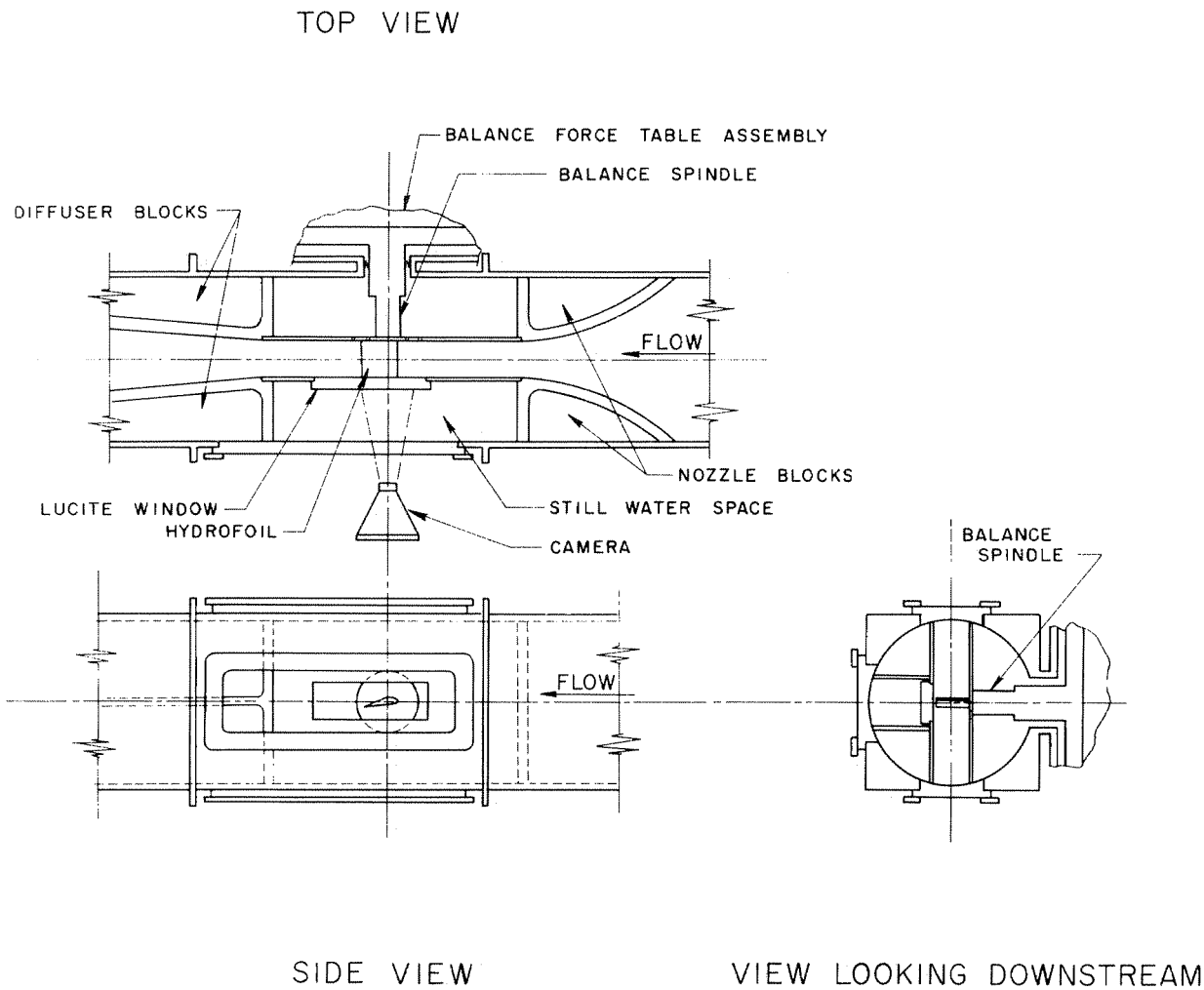

Fig. 3 - Schematic diagram of the water tunnel working section.

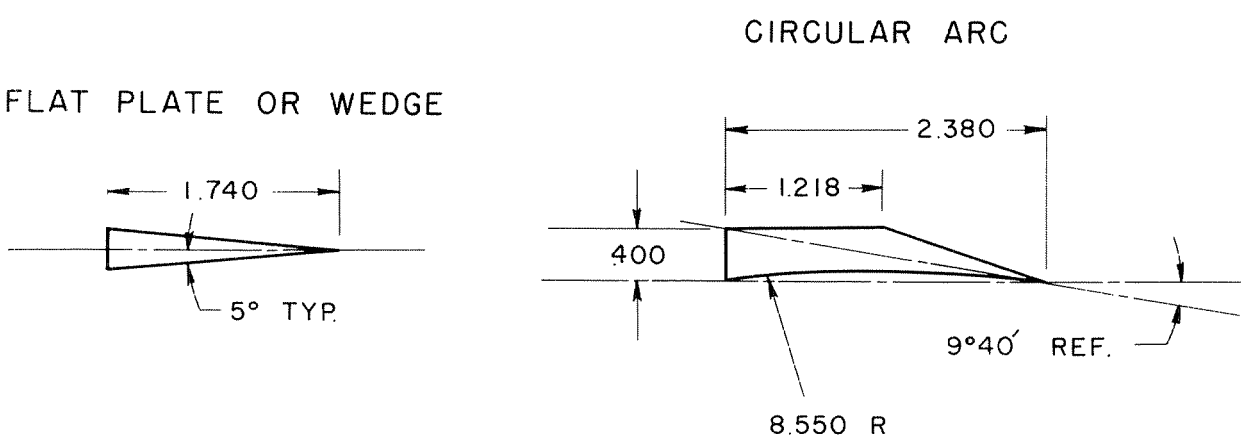

Fig. 4 - The two hydrofoil sections tested.

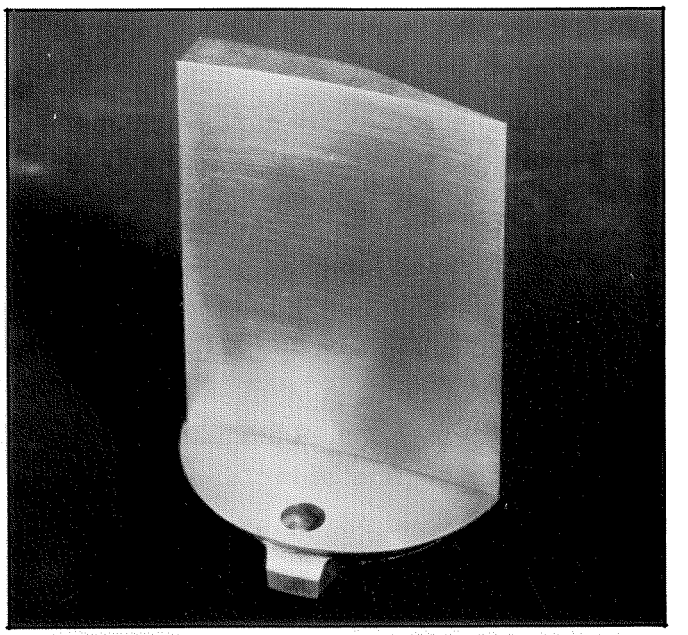

Fig. 5 - The circular arc hydrofoil ready for installation in the test section.

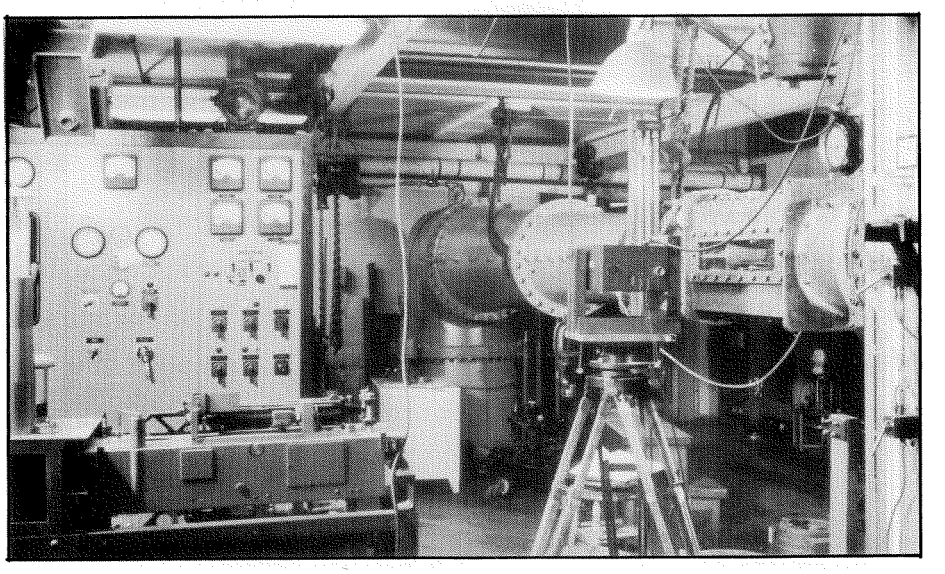

Fig. 6 - General arrangement of experimental apparatus.

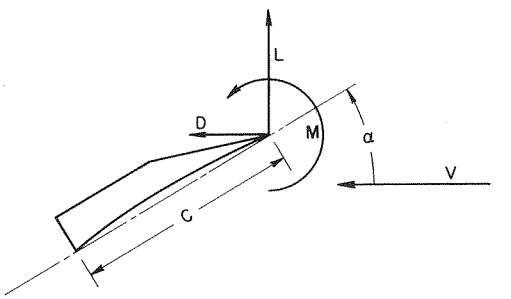

Fig. 7 - Conventions for positive forces and moments.

In these equations, A is the plan-form area of the model, c is the profile chord, V is the free stream velocity in the two-dimensional section and ρ is the density of water. The positive sense of all forces and moments is given in Fig. 7. The pitching moment is referred to the point at the profile leading edge.

The dynamic pressure $1/2\ \rho\ V^2$ was determined by measuring the static pressure difference between the water tunnel settling section and the upstream piezometer ring of the circular test section. This reading, from a carbon tetrachloride and water manometer, was converted into the dynamic pressure in the two-dimensional test section by simple area ratio considerations.

It was also necessary to determine the cavitation number for all runs. For full cavity flows which permitted direct measurement of p_k, the static pressure inside the cavity, the cavitation number is given by

$$K_k = \frac{p_o - p_k}{\frac{1}{2}\rho V^2} \quad .$$

The symbol p_o represents the free stream static pressure in the two-dimensional test section. For flow states which did not permit the direct measurement of the cavity pressure, the cavitation number was based upon p_v, the vapor pressure of water at the given temperature. For these cases the cavitation number is given by

$$K_v = \frac{p_o - p_v}{\frac{1}{2}\rho V^2} \quad .$$

The free stream static pressure p_o was measured by means of a mercury barometer which is connected to the piezometer ring at the upstream end of the circular working section. This reading was converted to the two-dimensional channel static pressure by taking account of known friction losses[3] and the area ratios between the two points. The cavity pressure p_k required two measurements for its determination. First, a U-tube mercury manometer was used to measure the difference between the cavity pressure and the barometric

pressure outside the tunnel. Second, the barometer was read. The cavity pressure is obtained by subtracting the U-tube reading from the barometer reading.

For each data point the state of cavitation on the model was photographically recorded and the gap between the working section wall and the free end of the model was adjusted to within .002 inch clearance. This last precaution has been found necessary to keep the effects of the end gaps negligible.

EXPERIMENTAL RESULTS

In this section we shall consider many special aspects of our experimental findings. Since it is impractical to present all of the data in these discussions, we have tabulated in the appendix to this report the experimental values of lift coefficient C_L, drag coefficient C_D, pitching moment coefficient C_M, and the cavitation numbers K_k and K_v for each run. For convenience, the lift-drag ratio is also given for each run. A run is identified by the number assigned to the photographic exposure which recorded the state of cavitation on the profile. In the tables this is called the "Film number". In each table the data are grouped according to attack angle. In Table I for the flat plate or wedge, the angle α_c between the flow direction and the face which opposes the flow (rather than the wedge centerline) is used as the basis for arranging the table. In Table II the attack angle α is measured with respect to the chord of the circular arc segment which forms the lower surface of the profile (cf. Fig. 7). The attack angle for the bent plate data of Table III is measured from the chord line which passes through the sharp leading edge and through the rear corner of the upper surface of the circular arc profile. When the runs for the bent plate configuration were made, the circular arc model was tested at -14, -16, -20, -30, -45 and -60 degrees referred to the circular arc chord line. The bent plate chord line is $9^\circ 40'$ from the circular arc chord line so that the entries in Table III are in the range of α from $23^\circ 40'$ to $69^\circ 40'$. It may be seen that some of the tabulated values of

K_k are marked with an asterisk. Entries so marked may be questionable, because the small cavities were foamy rather than clear and steady so that the cavity pressure could not always be reliably measured. However, it was found by comparison with other data in a group that the asterisked values of K_k more often than not represent consistent data points. In all tables the coefficients represent the average of ten individual force or moment readings. The ten readings seldom showed appreciable deviations from each other.

As mentioned previously, data were taken for various cavitation numbers at fixed attack angles. Typical runs gave plots of lift, drag, and pitching moment coefficients as functions of cavitation number. Examples of the data from flat plate and circular arc experiments are shown in Figs. 8, 9 and 10.

In Fig. 8, C_L, C_D, and $-C_M$, for the flat plate at $\alpha_c = 12^o$, are shown plotted against the cavitation number. Some of the photographs which recorded the state of cavitation on the profile are also shown for certain points. These pictures show that as the cavitation increases, the lift, drag, and moment increase in magnitude until the cavity envelops the entire upper surface of the wedge. Then as the cavity continues its growth and becomes a large clear cavity, the magnitudes of the forces and moment decrease steadily. It is interesting to note that there must be a considerable amount of cavitation on the upper surface of the wedge before appreciable changes in the forces are produced. Moreover, in the regime of flow to the left of the peak coefficients, the steady full cavity flows produce very steady hydrodynamic forces. In the region to the right of the peak, the flow is not as steady and the resulting forces tend to fluctuate. The severity of these fluctuations appeared to depend on the nature of the noncavitating flow. For example, if the profile acts like a stalled airfoil with severe buffeting in noncavitating flow, then the forces on the profile in partially cavitating flow (to the left of the peak) are likely to fluctuate severely. The frequency response of the force readout equipment did not permit quantitative data to be taken on these force fluctuations.

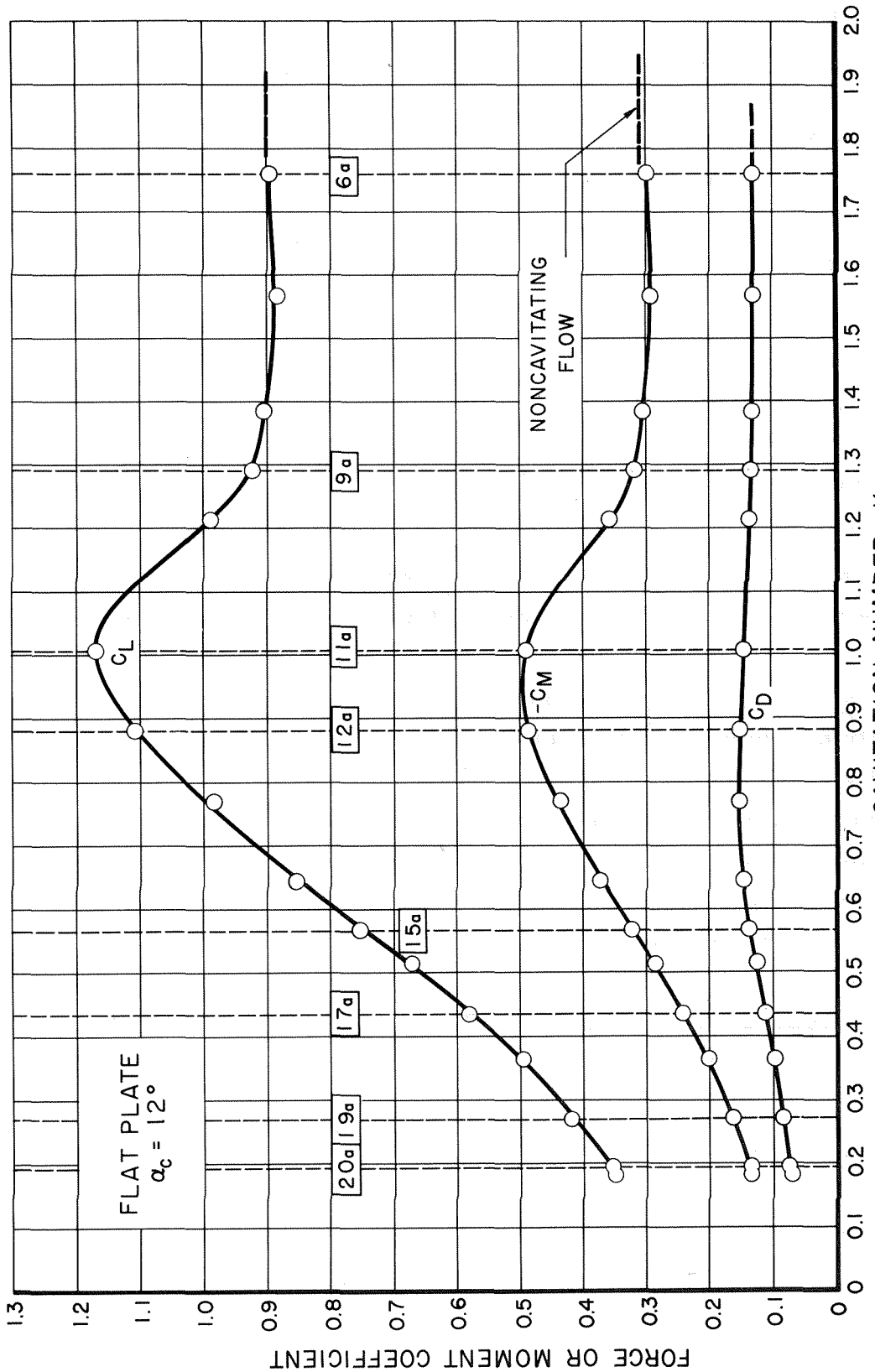

Fig. 8a - The effects of cavitation on the forces and moments of the flat plate at an attack angle of 12°. The numbered dotted lines which pass through the various data points correspond to the numbers on the photographs of Fig. 8b.

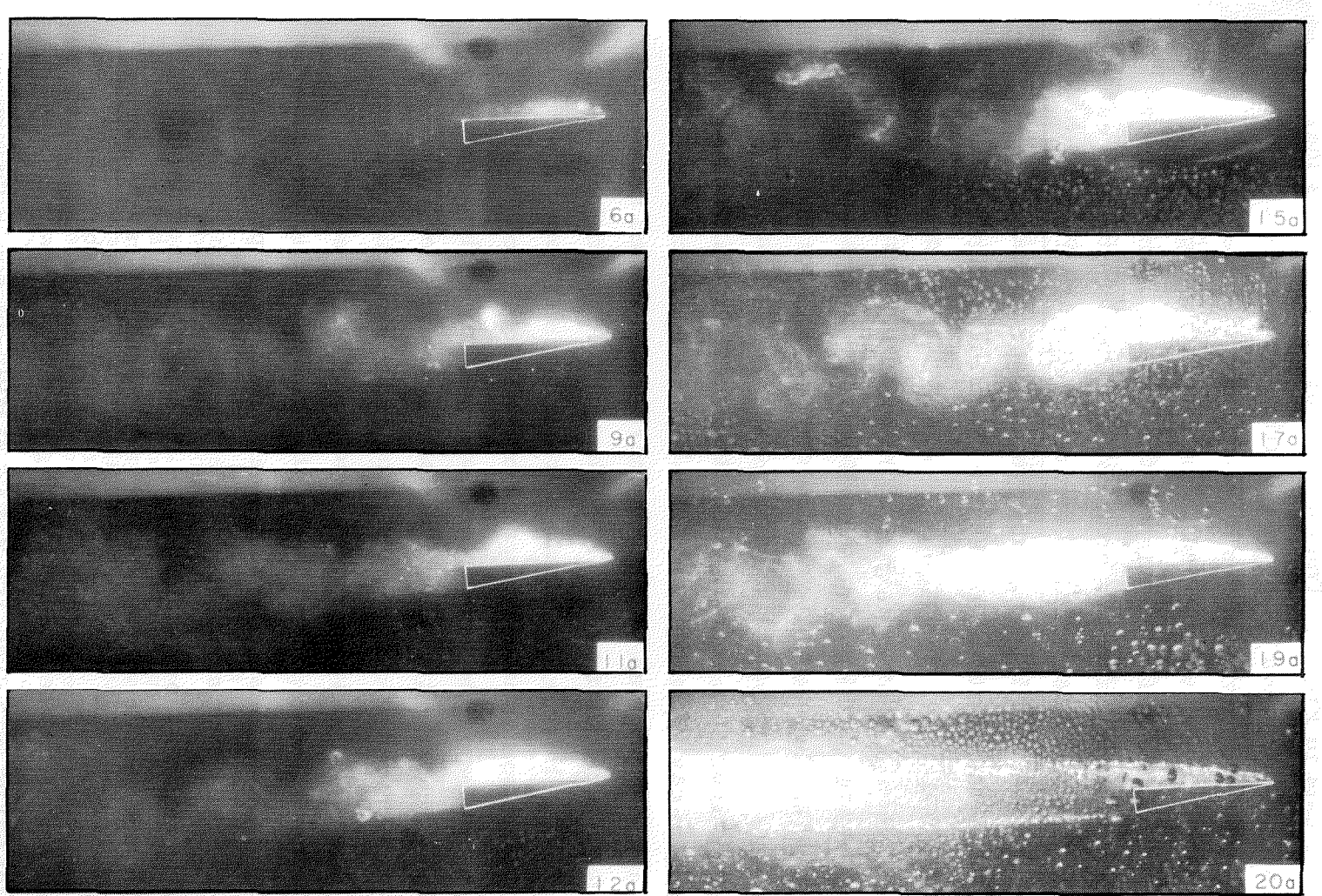

Fig. 8b - The development of cavitation on the flat plate hydrofoil. Each photograph corresponds to the data so numbered in Fig. 8a. The air bubbles which partly obscure the pictures taken at the lower cavitation numbers result from the diffusion of air into bubbles trapped in the still water space between the channel wall and the outer working section window (see Fig. 3). These 5 microsecond photographs show the instantaneous structure of the cavity and the wake. These are indications of a Karman street in the wake behind the cavity.

Figure 9 presents the results of experiments on the circular arc profile at $\alpha = 10^{o}$. The data exhibits the same general trends as the plot of flat plate data in Fig. 8. Thus we see for both sections that the forces reach a peak when the profile is first completely enveloped by cavitation and as the cavity grows the forces steadily decrease in magnitude. Moreover, we see that in the full cavity regime the cavity extends from the sharp leading and trailing edges and that for both the flat plate and circular arc profiles, only the lower surfaces are exposed to flowing water. This situation obtains at all attack angles which are sufficiently high. However, in certain ranges of low attack angles, the cavity flows assume different configurations. For example, at angles α_c under 7^{o}, the flat plate profile behaves like a slightly pitched wedge with the cavity springing from the two downstream corners. That is, we found that the flow does not separate from the sharp leading edge until the centerline of the wedge makes an angle of 2^{o} with the flow direction. The circular arc profile being of more complex geometry than the wedge permits a greater variety of cavity configurations at low attack angles. An example of such a flow is given in Fig. 10 where the force and moment coefficients for the circular arc at $\alpha = 0^{o}$ are plotted against the cavitation number. Here we see that, as cavitation develops on the profile, it behaves somewhat like a cambered section which produces a positive lift. But upon the development of a full cavity flow, the section becomes equivalent to a flat plate at a negative attack angle. Thus, the lift and moment change sign twice as the cavitation number decreases. Although this irregular behavior may be augmented by the abrupt corner in the upper surface of the profile used in the present experiments, it seems likely that other sharp-edged profiles with smooth convex upper surfaces would experience much the same sort of force reversal at low attack angles. When the attack angle of the circular arc profile was increased, additional full cavity flows were observed. At $\alpha = 4^{o}$ a full cavity sprang from the abrupt corner of the upper surface and the trailing edge of the lower surface, while a partial cavity was observed to extend from the sharp leading edge part way back along the lower surface. At $\alpha = 7^{o}$ the partial

cavitation on the lower surface was suppressed and a full cavity sprang from the corner in the center of the upper surface and the trailing edge of the lower surface. At $\alpha = 9^{o}$ we observed the first signs of cavitation extending from the sharp leading edge along the upper surface of the profile. However, this small cavity was still distinct from the large full cavity which originated from the trailing edge of the lower surface and from the corner in the center of the upper surface. The lowest angle for which the full cavity was observed to spring from the leading and trailing edges of the lower surface of the circular arc profile was $\alpha = 10^{o}$.

As was noted in our discussion of Figs. 8 and 9, there is generally a peak in the magnitude of the forces when the upper surface of the profile becomes entirely enveloped by cavitation. The relative magnitudes of the increase in lift and moment over their values in noncavitating flow are generally quite large as long as the attack angle is kept reasonably low. However, the drag coefficient does not show such a marked change. This state of affairs appears to be due to the fact that the present profiles are not intended to operate efficiently in noncavitating flow. The blunt trailing edge of both models gives rise to high drag coefficients and to low lift coefficients in fully wetted flow. Therefore, the onset of cavitation is probably far more beneficial to the development of lift on these profiles than it would be for sharp-edged profiles of clean aerodynamic shape. On the other hand, the increase in drag occasioned by the development of cavitation on clean sharp-edged profiles should be much more pronounced than is the case for the present profiles.

Finally, we note that in plotting the data of Figs. 8, 9, and 10, we have used both the cavitation numbers K_k and K_v. The cavitation number, based on cavity pressure K_k, was used wherever its measurement was possible. In those instances where this could not be done, the cavitation number, based on vapor pressure K_v, was used as the basis for the plot. In most instances this procedure has resulted in the data to the right of the peak being plotted as a function of K_v while nearly all of the data at the lower cavitation numbers are plotted against K_k. The justification for this procedure which has been

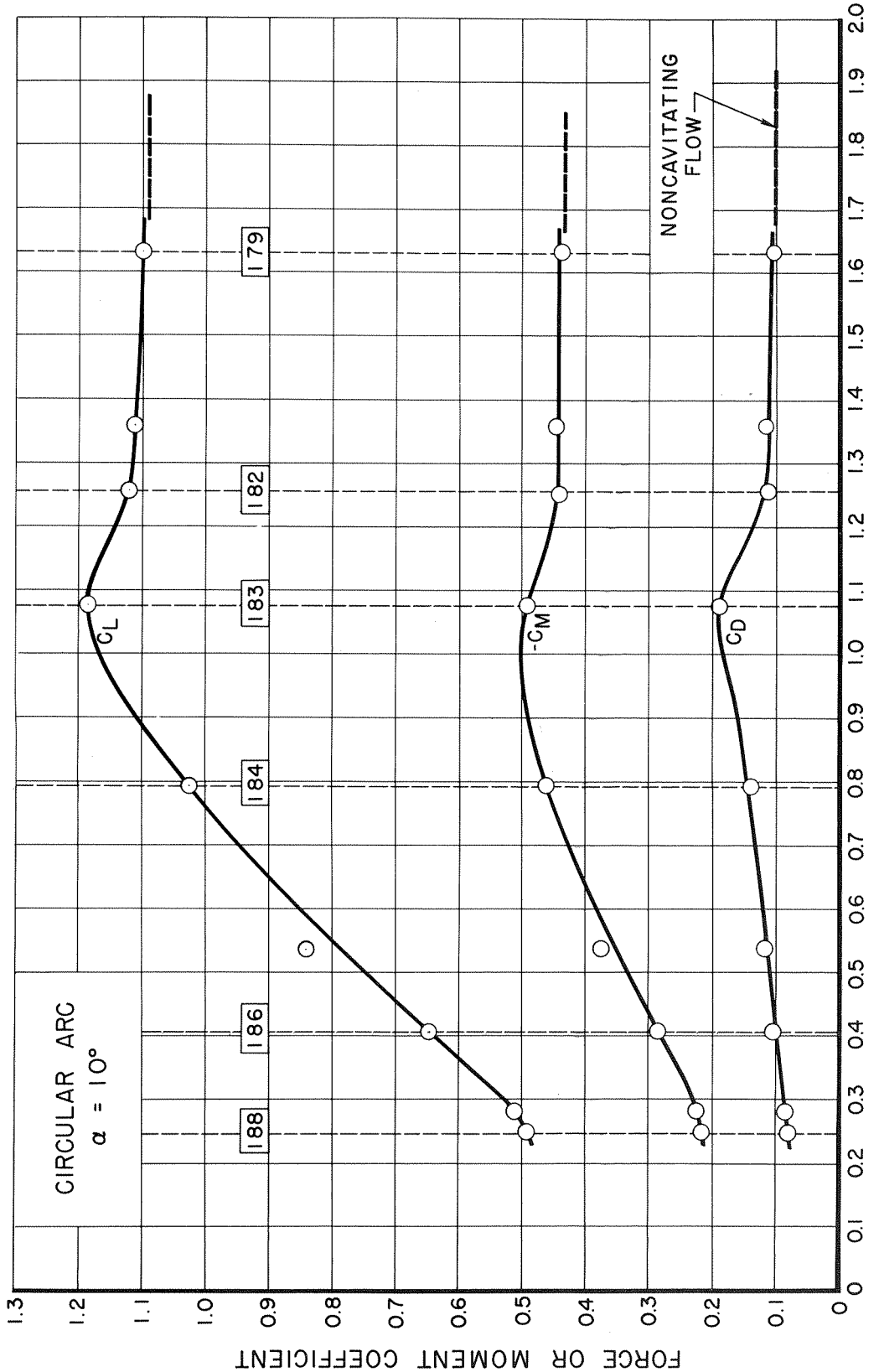

Fig. 9a - The effects of cavitation on the forces and moment of the circular arc hydrofoil at an attack angle of 10^{o}.

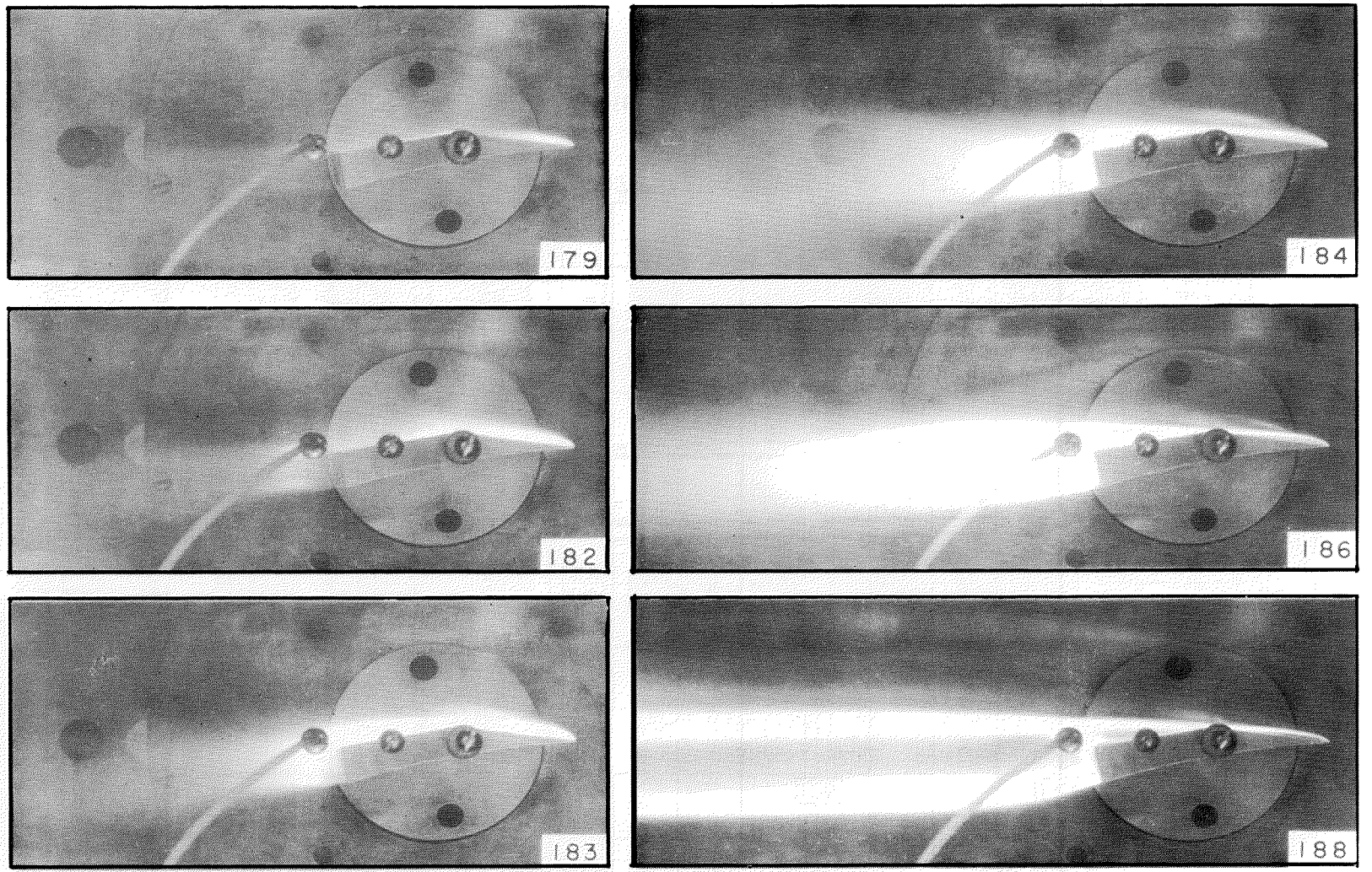

Fig. 9b - The development of cavitation on the circular arc profile at $\alpha = 10^{\circ}$. These time photographs show an average outline of the cavity. The tubing shown in the pictures connects the probe used to measure the cavity pressure with a mercury manometer outside the tunnel. This tubing is in the still water space and the probe is a short length of 1/16 dia. brass tube projecting into the cavity from the lucite window of the two-dimensional channel.

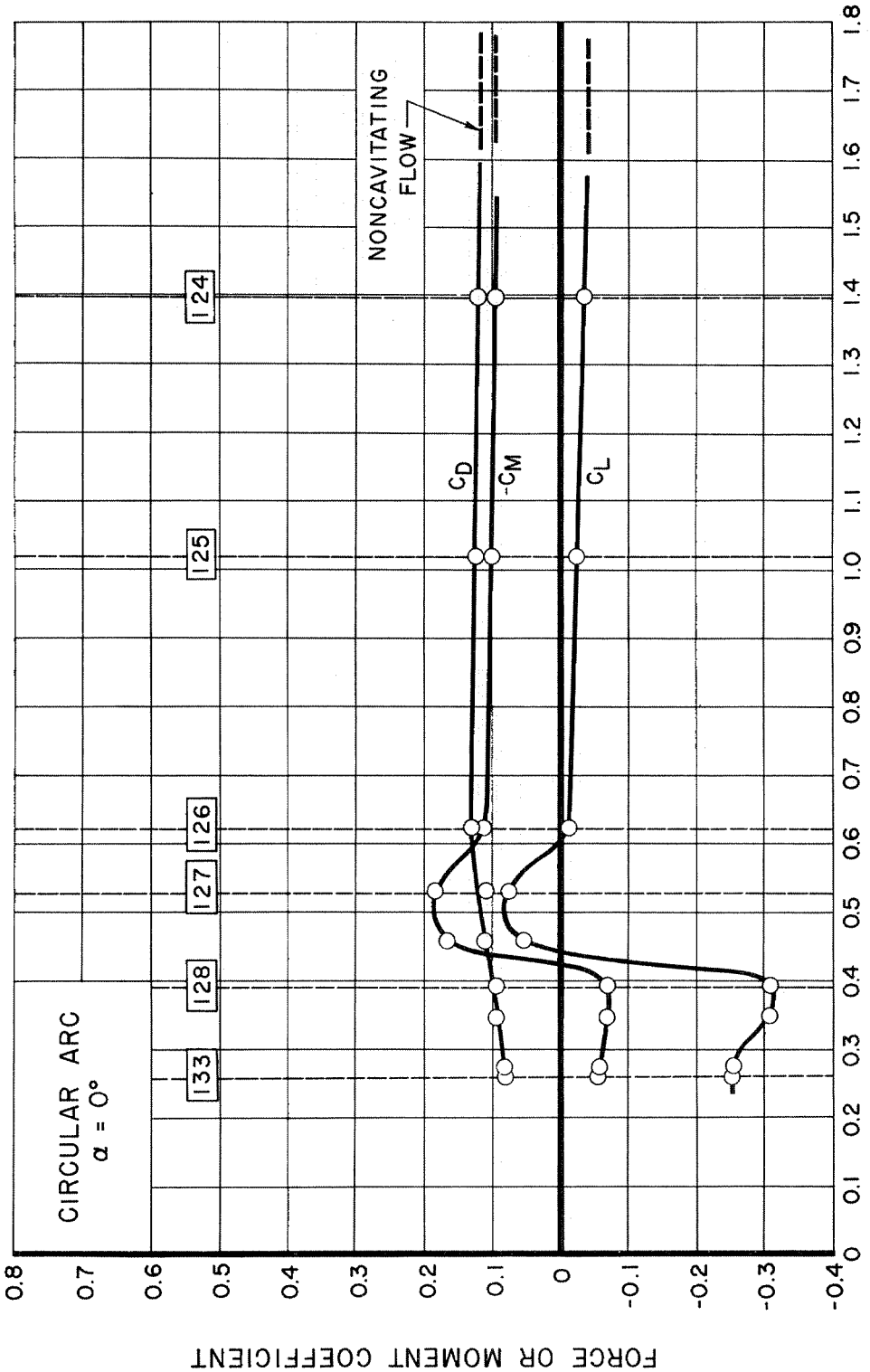

Fig. 10a - The effects of cavitation on the forces and moment of the circular arc hydrofoil at an attack angle of 0°.

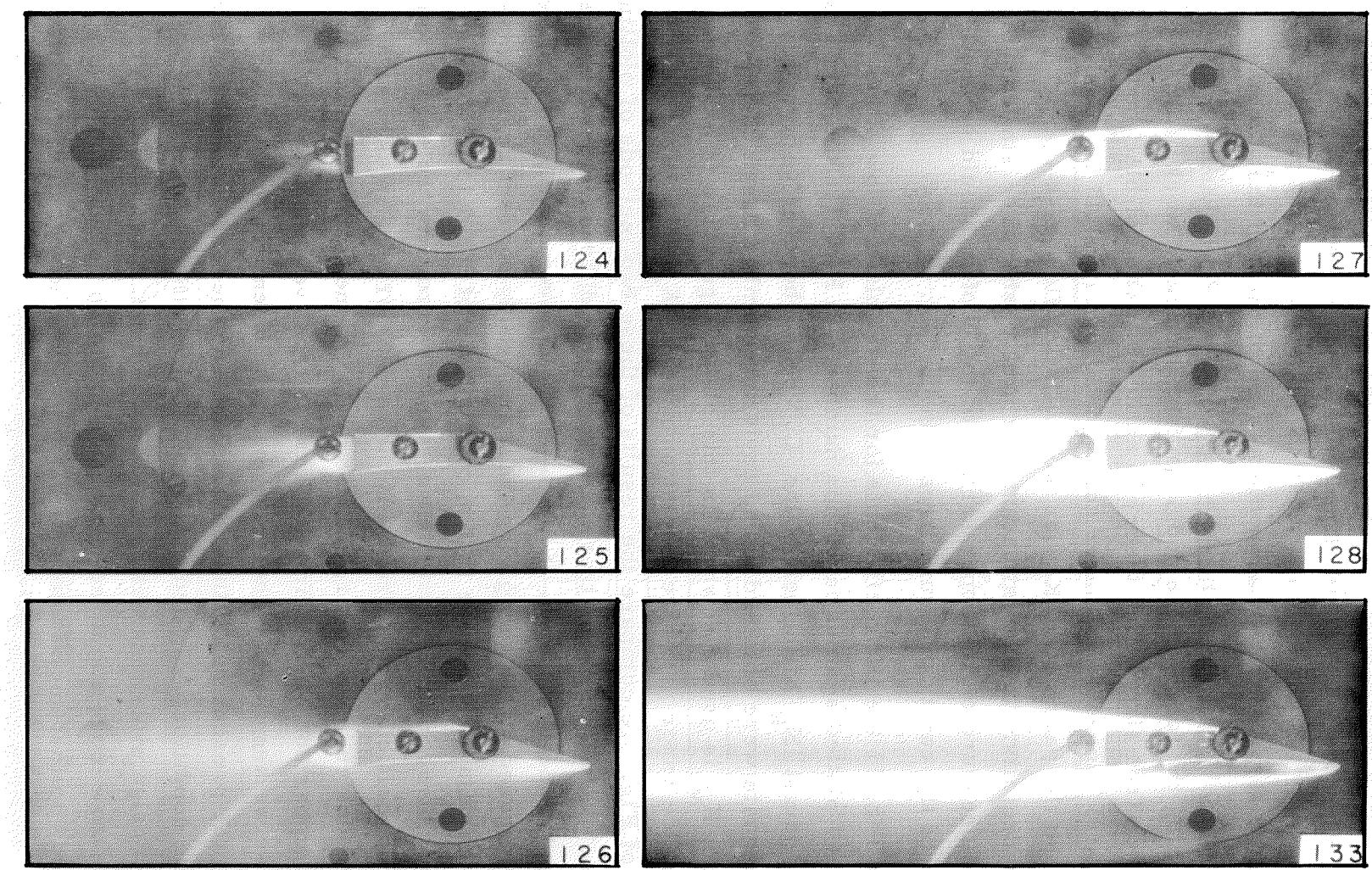

Fig. 10b - The development of cavitation on the circular arc profile at $\alpha = 0^{o}$.

followed throughout the present work, originates from the well-known results of Reichardt[5] which showed that the cavity geometry and the drag force for a given axially symmetric body in full cavity flow is determined by the cavitation number K_k based on cavity pressure. This result is physically reasonable in view of the fact that the base pressure for such bluff body flows is certainly a primary factor in determining the force on the body. In fact the recent work of Roshko[6], which uses free streamline theory in an investigation of bluff body drag in air, suggests that under some conditions it might be consistent to use the parameter K_k for noncavitating flow past sharp-edged hydrofoils. In such situations the profile should be stalled and the base pressure on the upper surface of the profile should be used in place of the cavity pressure in calculating K_k.

In Fig. 11 the lift coefficients for the flat plate at low attack angles are plotted against cavitation number. In Fig. 11a the data are plotted against K_k to the left of the C_L peak wherever valid cavity pressure data were obtained. The cavitation number based on vapor pressure K_v is used elsewhere in this plot. Figure 11b is based entirely on the vapor pressure cavitation number K_v. The superposed curves of Fig. 11c compare the results of these two methods of plotting the data. As can be seen, there is a consistent difference between the two representations of the data. If for the reasons given above, we consider the curve based on K_k as giving the more nearly correct representation of the data, we can see that in applications of the data to design situations involving full cavity flows, serious errors in the estimation of the lift coefficient could result if the parameter K_v is used as a basis for design. Moreover, the use of K_v alone may not permit the direct comparison of experimental results from various test facilities. Of course we assume that the relationship between K_v and K_k implied by the present water tunnel tests does not necessarily hold under full scale conditions. In order to apply the results of water tunnel tests to design situations with greater confidence, it would be of great value to know more about the mechanics by which full cavity flows are sustained, so that such factors as air diffusion and turbulent entrainment

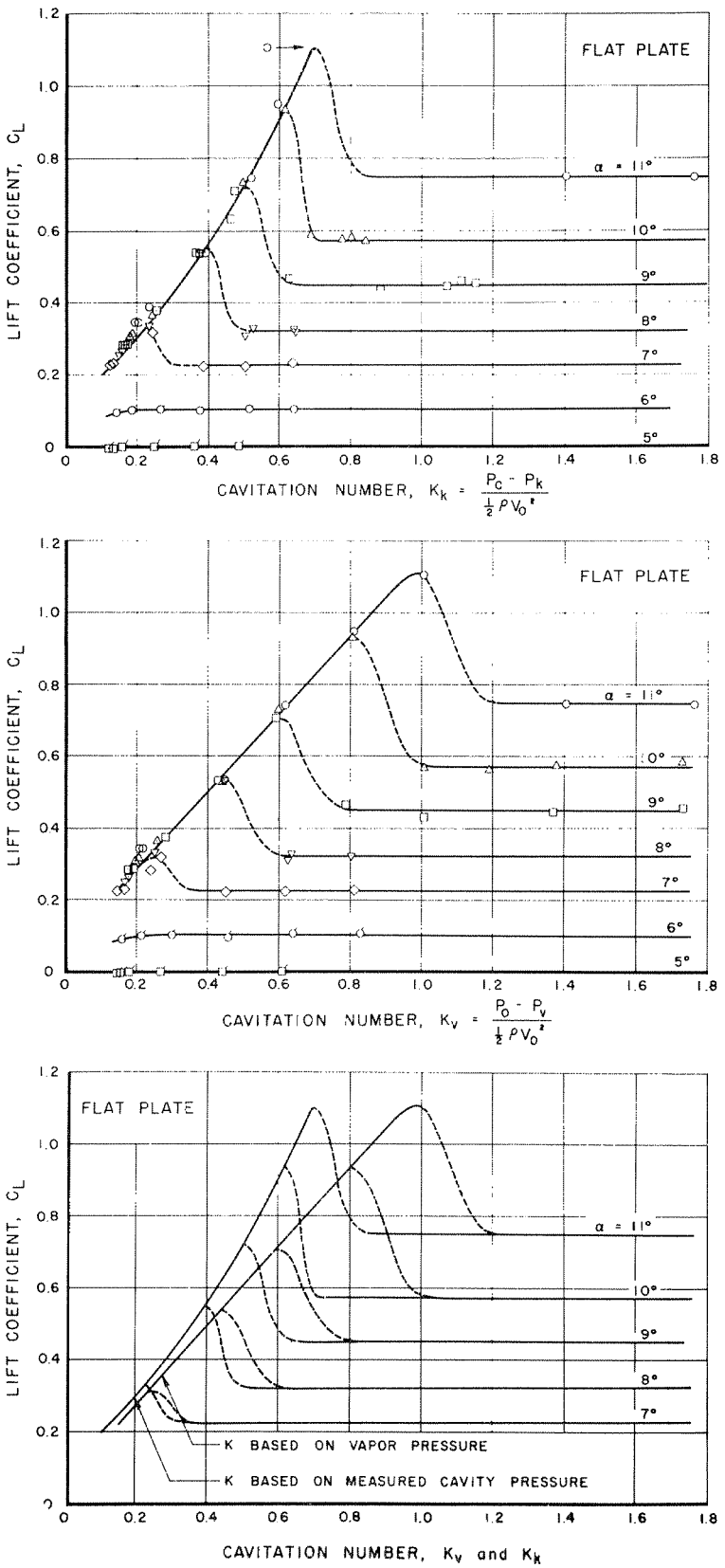

Fig. 11 - The effect of different expressions for the cavitation parameter on the appearance of the force data is shown.

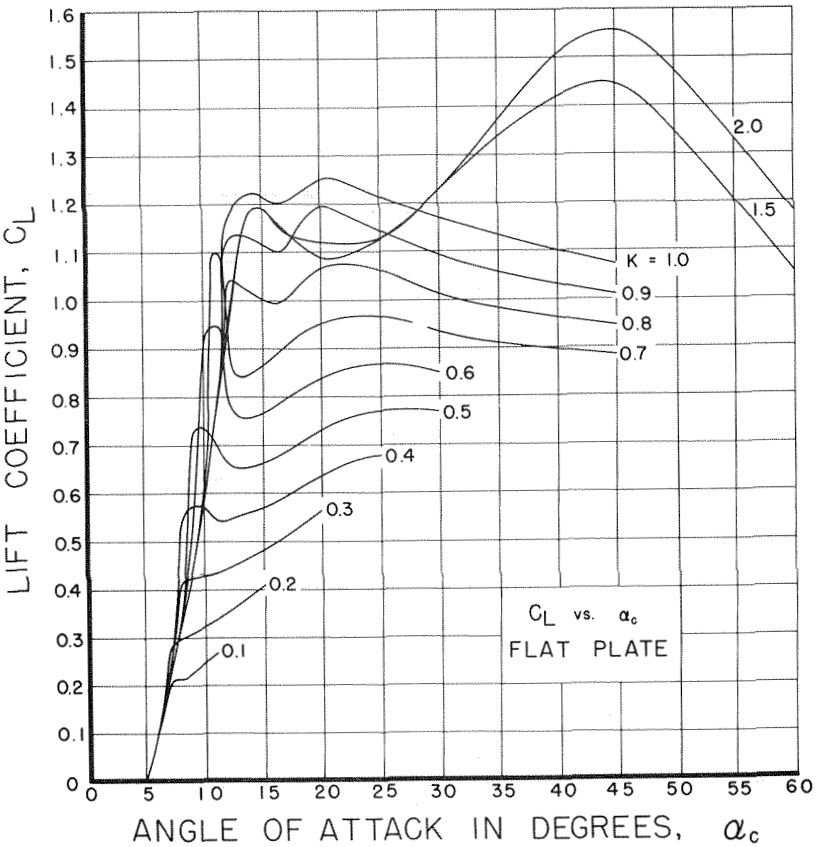

Fig. 12 - C_L vs α_c for the flat plate hydrofoil.

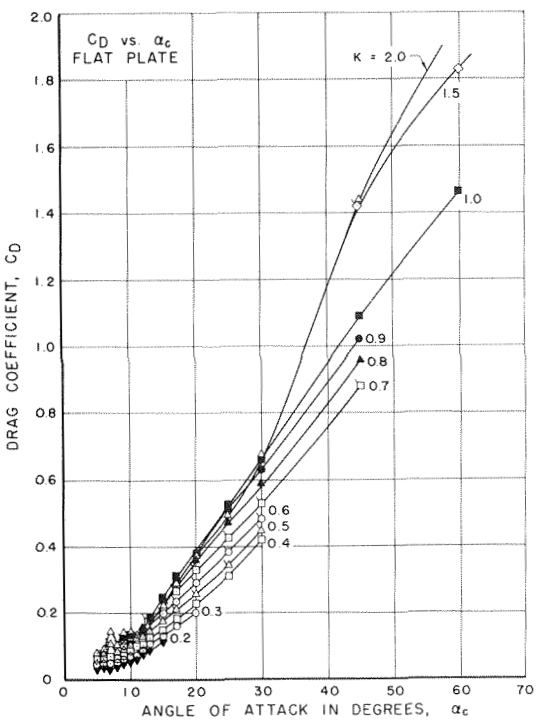

Fig. 13a - C_D vs α_c for the flat plate hydrofoil.

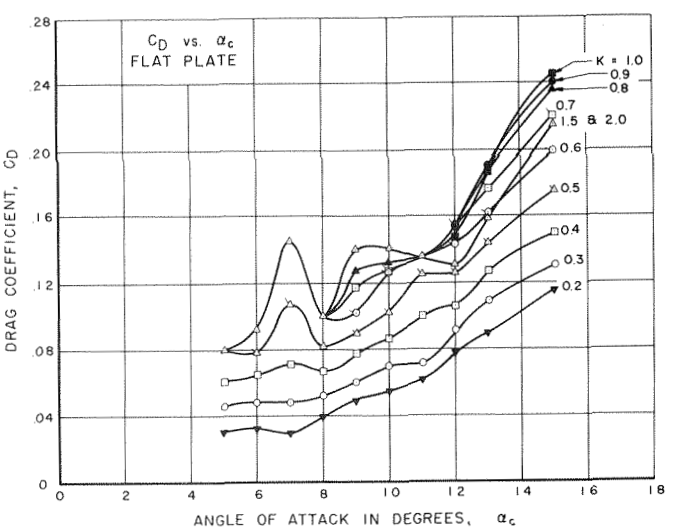

Fig. 13b - C_D vs α_c for the flat plate hydrofoil at the lower attack angles.

can be accounted for. Definite answers to the applicability of water tunnel results and the estimation of K_k from given design data must await further investigations. For the present it would seem that significant errors could occur at the higher values of the cavitation number. For cavitation numbers below 0.3, say, it would appear that the use of either K_v or K_k might be expected to give results which are within engineering accuracy.

All the experimental results of Tables I, II, and III were plotted against cavitation number in the manner of Figs. 8, 9, and 10. The curves which were faired through these data then formed the basis for cross plots in which the cavitation number appears as a parameter which defines the individual members of various families of curves. As explained above, wherever possible the cavitation number in these plots is based on the cavity pressure. It should be emphasized that the points which are indicated on these cross plots are taken from curves which have been faired through the experimental data. They are not experimental points and are included on the cross plots to facilitate their use. The points on the cross plots are arranged so that each cavitation number is denoted by its own symbol.

A complete set of curves for the flat plate profile is given in Figs. 12 through 18. For selected values of the cavitation number, families of curves giving C_L, C_D, C_M and L/D versus α_c are plotted in Figs. 12 through 15. From Figs. 12 and 14 we see that the family of curves for C_M looks somewhat like the reflection of the C_L family of curves in the horizontal axis. This is to be expected because the origin of moments is taken at the profile leading edge. If the present data for C_L, C_D, and C_M are used to calculate the center of pressure location, we obtain curves showing the travel of the center of pressure with changing cavitation number. In Fig. 15a the distance of the center of pressure from the leading edge is plotted against the cavitation number for runs at $\alpha_c = 12^o$ and 7^o. The center of pressure distance is expressed as a fraction of the profile chord length. The points for the curve labeled $\alpha_c = 12^o$ correspond to those of Fig. 8a with the result that the relationship between cavitation

development and center of pressure position may be determined with the help of Fig. 8b. As cavitation develops on the profile, the center of pressure moves from its position in noncavitating flow toward the rear of the profile. Then as the cavity becomes more fully developed, the center of pressure moves toward the nose. The general trend for the 7^{o} curve seems to fit into this pattern, but the cavitation number could not be lowered far enough to permit the region to the left of the peak to be investigated. It appears that the greatest change in center of pressure position with cavitation number is limited to 15% of the chord. In Fig. 15b the change in center of pressure position with attack angle is shown for a constant cavitation number. The curve is faired between those points for which the profile is in full cavity flow. The tendency of the center of pressure to move toward the center of the profile as α_c increases is evident.

For a fully cavitating flat plate at the attack angles tested, we may certainly neglect viscous forces in considering the variation of the lift-drag ratio with α_c. We might therefore expect the lift-drag ratio to be given by the cotangent of the attack angle since all pressures act in a direction normal to the plate. In Fig. 16 the cotangent curve is plotted as a dashed line in order to compare this rule with the experimentally determined values of L/D. We see that for sufficiently high α_c and for sufficiently low K the cotangent rule gives a good representation of the data. For lower α_c and higher K we see that L/D depends on the cavitation number. The peak in each L/D curve at constant cavitation number separates the full cavity flow state from the noncavitating or partially cavitating flow states. The profile was in full cavity flow for points to the right of each peak. The peaks in the L/D curves correspond to the sharp bends in the C_L and C_M curves of Figs. 12 and 14 where full cavity flows were found to exist to the right of each bend.

The cavitation polar diagram for the flat plate profile is given in Figs. 17a and 17b. As with the C_D vs α_c curves of Fig. 13, one plot represents the entire range of the data, and the other, plotted to a larger C_D scale, represents the data over the limited α_c range of greatest practical interest.

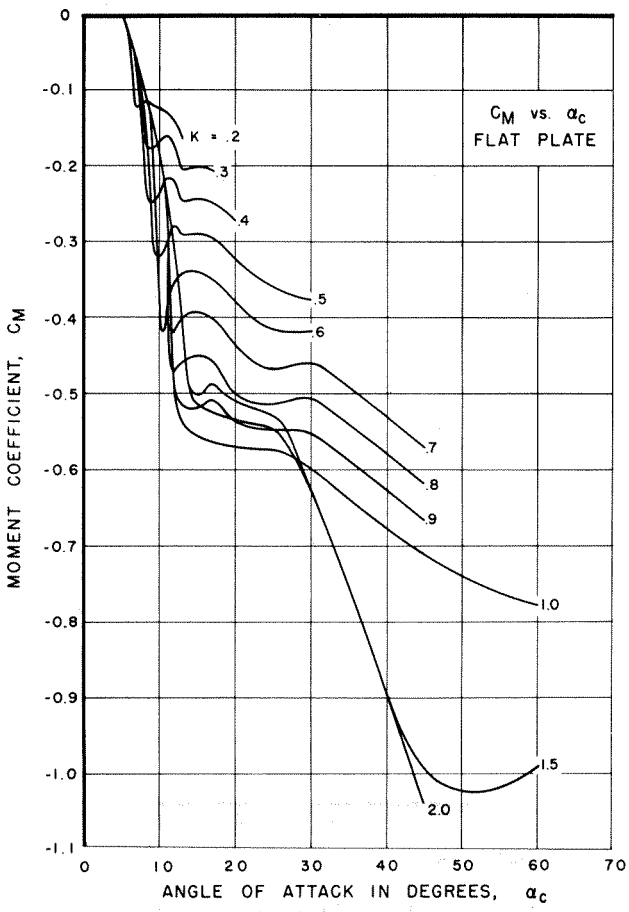

Fig. 14 - C_M vs α_c for the flat plate hydrofoil.

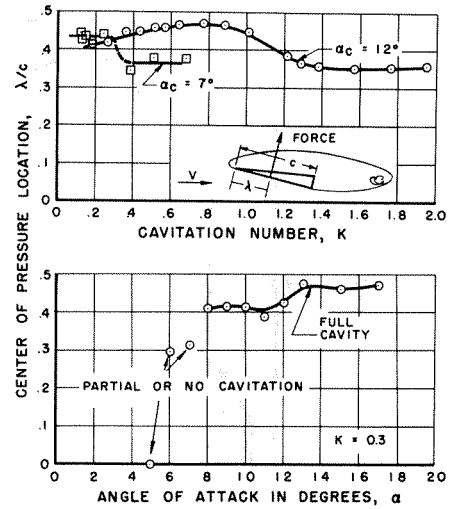

Fig. 15 - Center of pressure locations for the flat plate profile in full cavity flow.

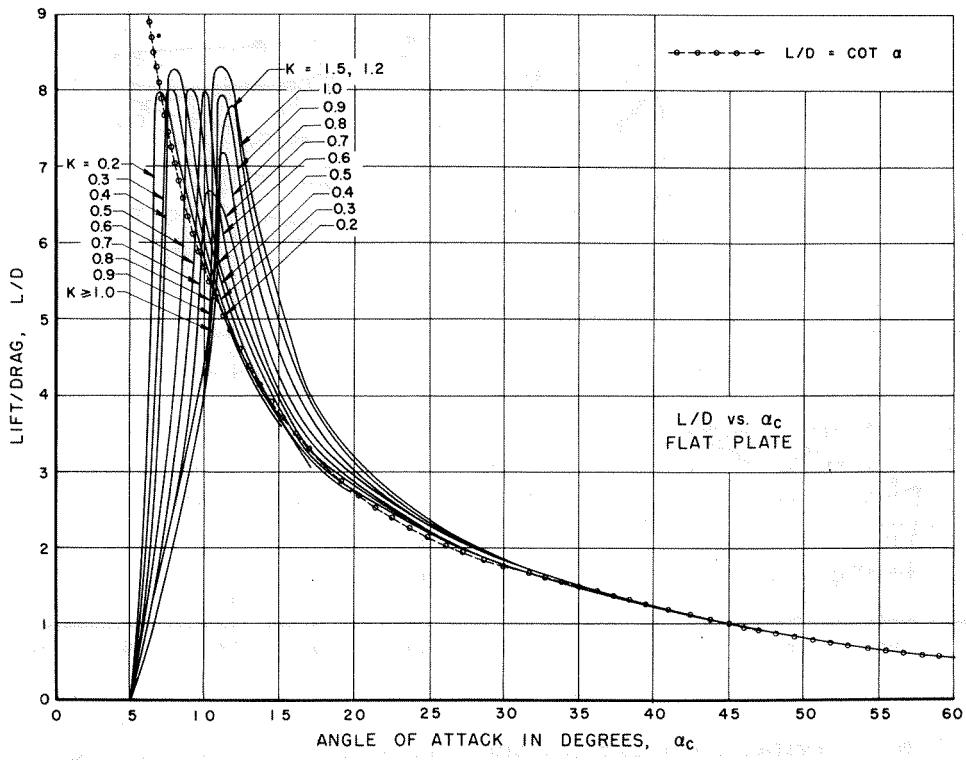

Fig. 16 - Lift-drag ratios vs α_c for the flat plate profile.

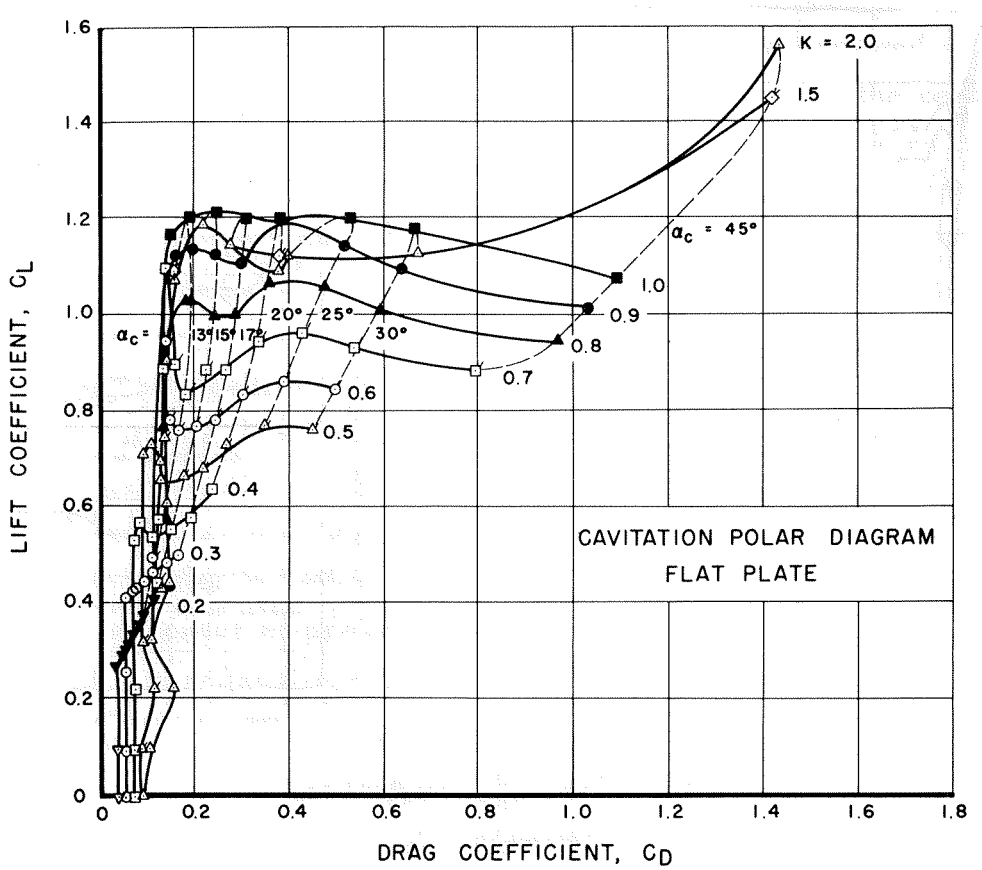

Fig. 17a - Cavitation polar diagram for the flat plate hydrofoil.

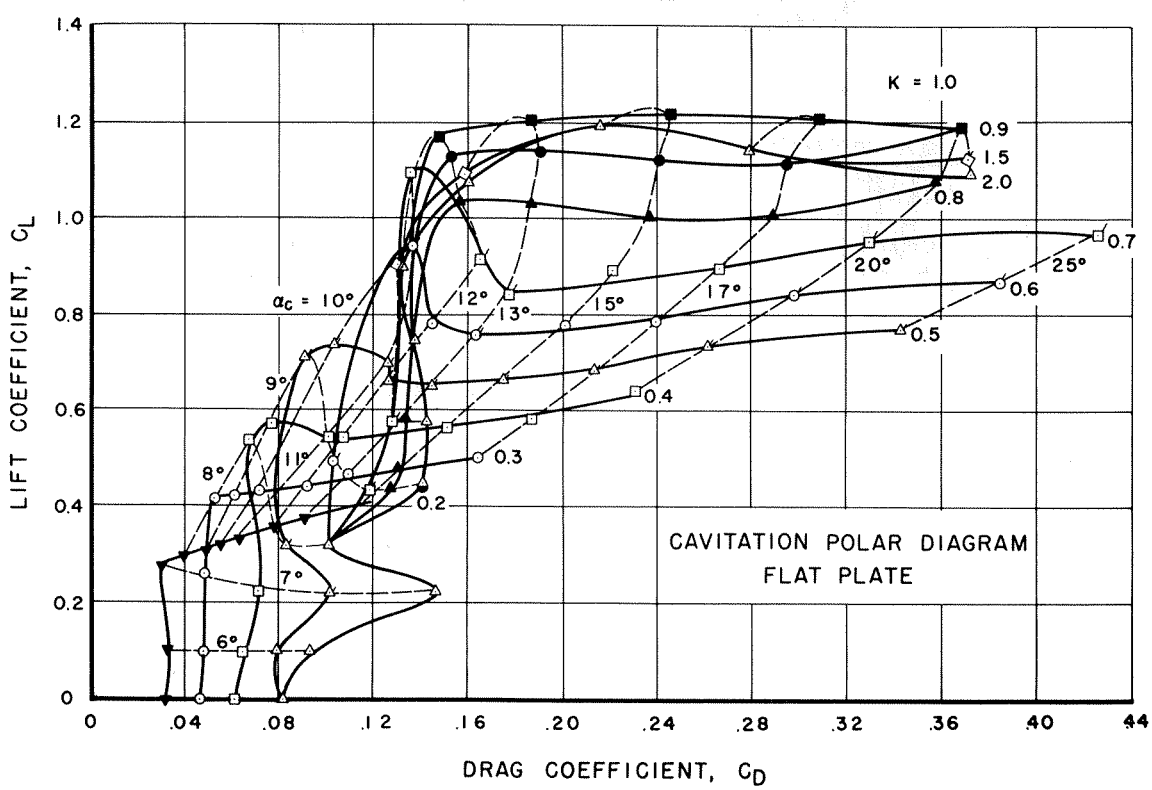

Fig. 17b - Cavitation polar for the flat plate hydrofoil at the lower attack angles.

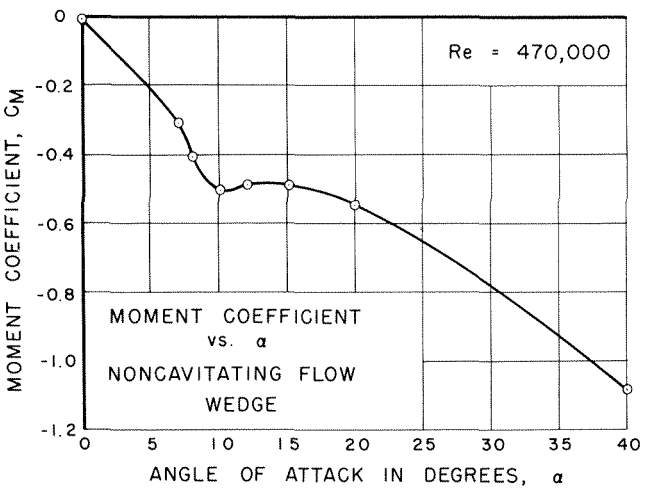

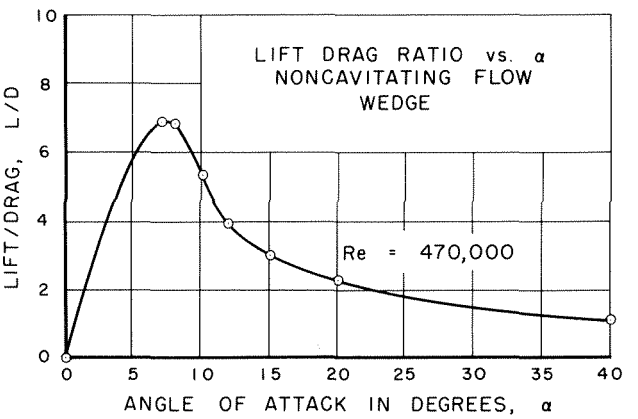

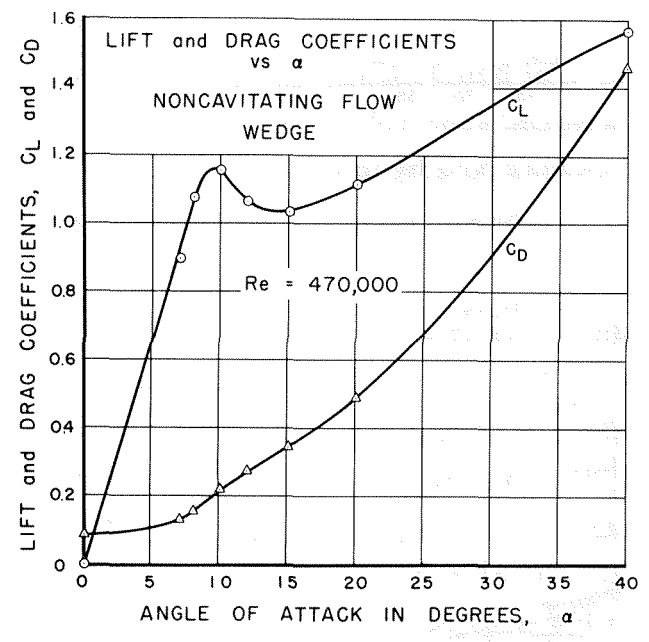

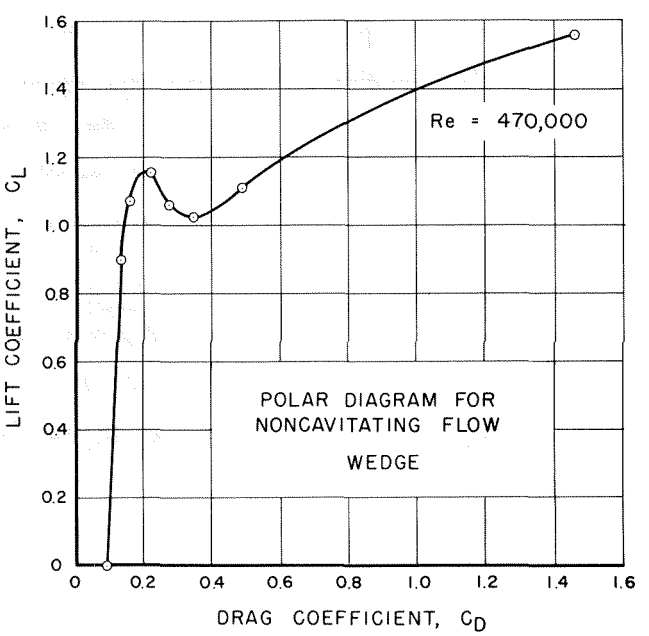

Fig. 18 - Hydrodynamic coefficients of the wedge profile in noncavitating flow.

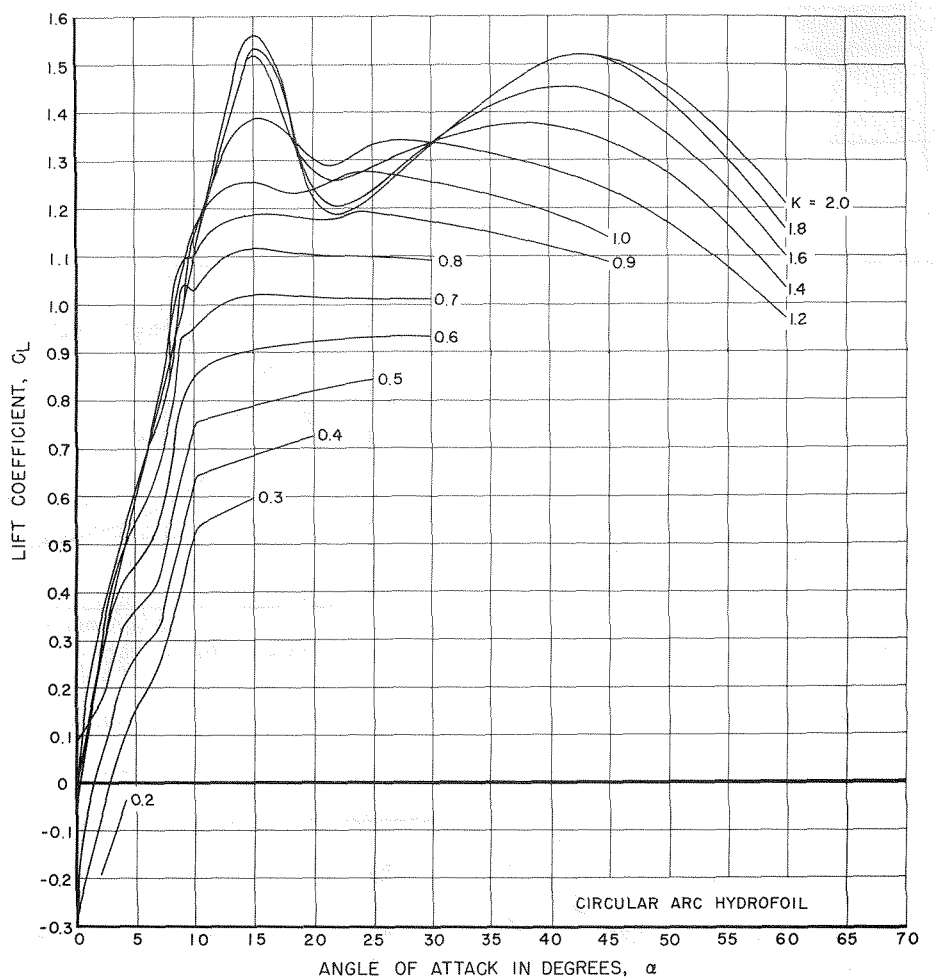

Fig. 19 - C_L vs α for the circular arc hydrofoil.

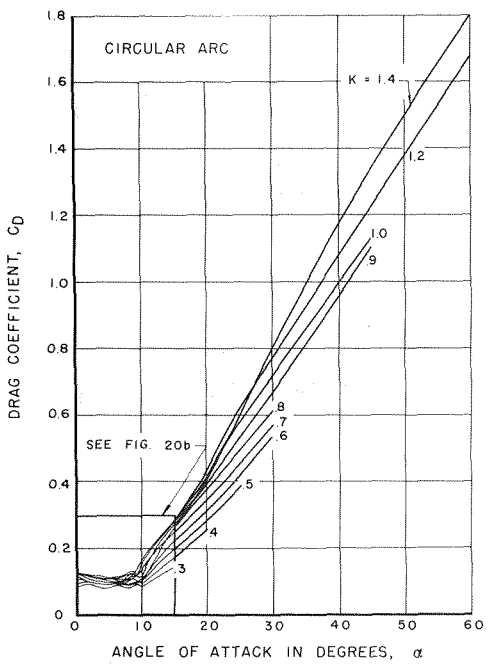

Fig. 20a - C_D vs α for the circular arc hydrofoil.

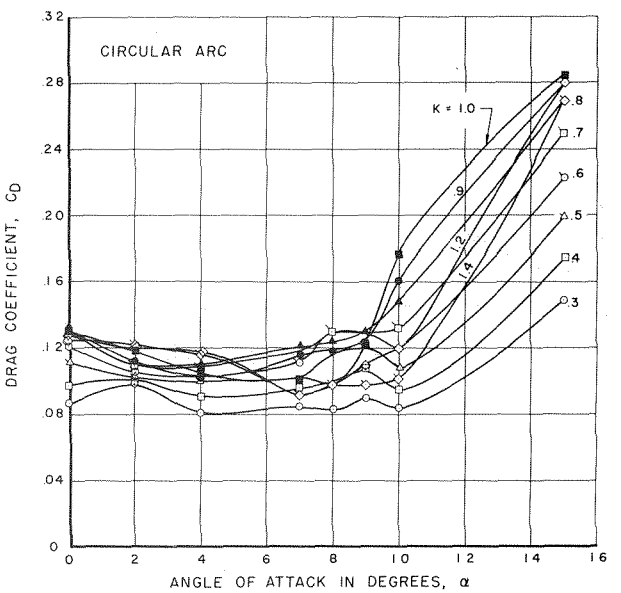

Fig. 20b - C_D vs α for the circular arc hydrofoil for the smaller values of α.

Finally, the experimental results for the wedge profile in fully wetted flow are given in Fig. 18. For these data the attack angle α is measured with respect to the wedge centerline so that the angle α and the angle α_c differ by 5^o.

Except for curves which involve the center of pressure position, the complete characteristics for the circular arc profile are presented in Figs. 19 through 24. This set of curves differs in no essential respect from the set of curves presented for the flat plate. Therefore the remarks made above for that profile will generally be applicable to the results for the circular arc. Of course there are certain detailed differences between the two sets of curves at low attack angles which are caused by the greater number of flow configurations attainable with the circular arc model in this range of α. This feature of the circular arc experiments has already been considered in connection with the discussion of Figs. 9 and 10. Of course there are other differences which may be ascribed to the effects of camber. In Fig. 22, which gives the lift-drag ratio for the circular arc as a function of α, the cotangent rule has also been included in order to permit an easier comparison with L/D results for the flat plate of Fig. 16. We see that the general features of the two sets of curves are similar and, in particular, we observe that the same trend for L/D with cavitation number exists for both profiles.

The effects of camber for high attack angles are given in Figs. 25 and 26 where values of C_L, C_D, C_M and L/D are presented for circular arc, flat plate and bent plate profiles in full cavity flows. The restriction to high angles ($\alpha = 25^o, 30^o$) was required because we found that cavitation occurred at the bend in the bent plate profile at lower angles. The penalty one incurs by changing from a concave to a convex hydrofoil is emphasized by the difference between the lift-drag ratios for the circular arc or flat plate profiles and the bent plate hydrofoil.

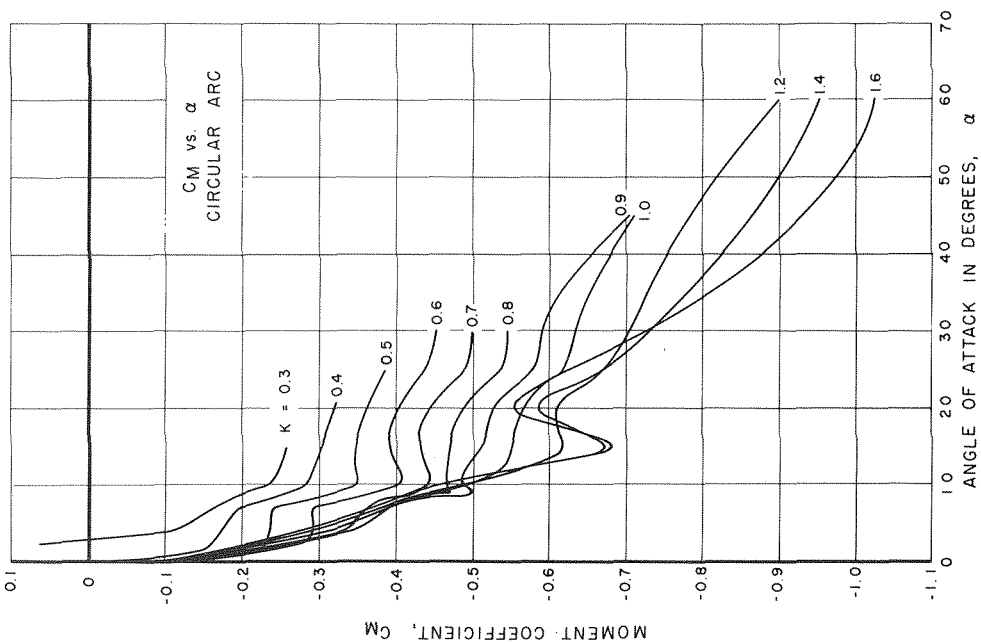

Fig. 21 - C_M vs α for the circular arc hydrofoil.

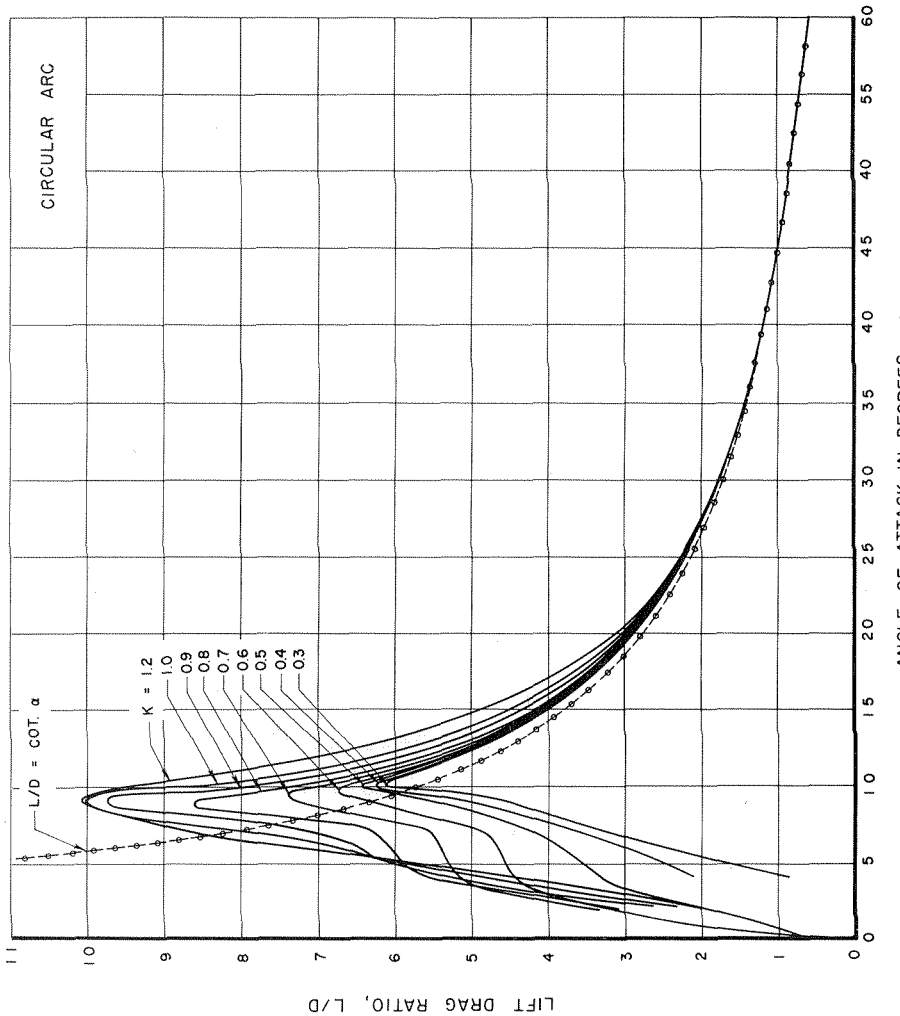

Fig. 22 - Lift-drag ratio vs α for the circular arc hydrofoil.

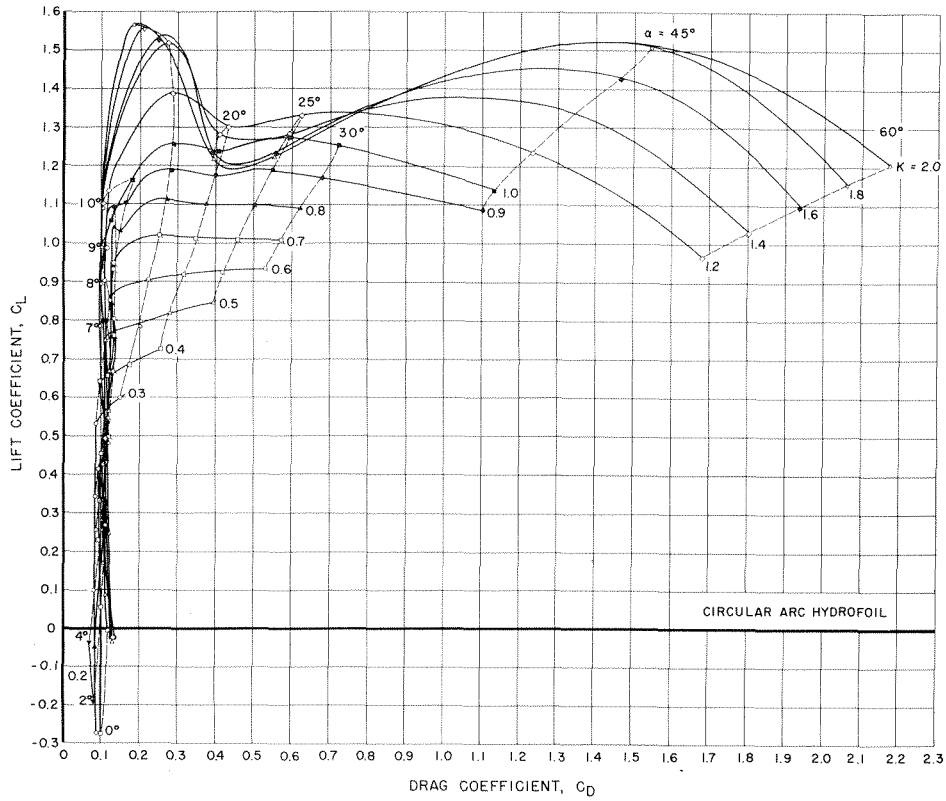

Fig. 23a - Cavitation polar diagram for the circular arc hydrofoil.

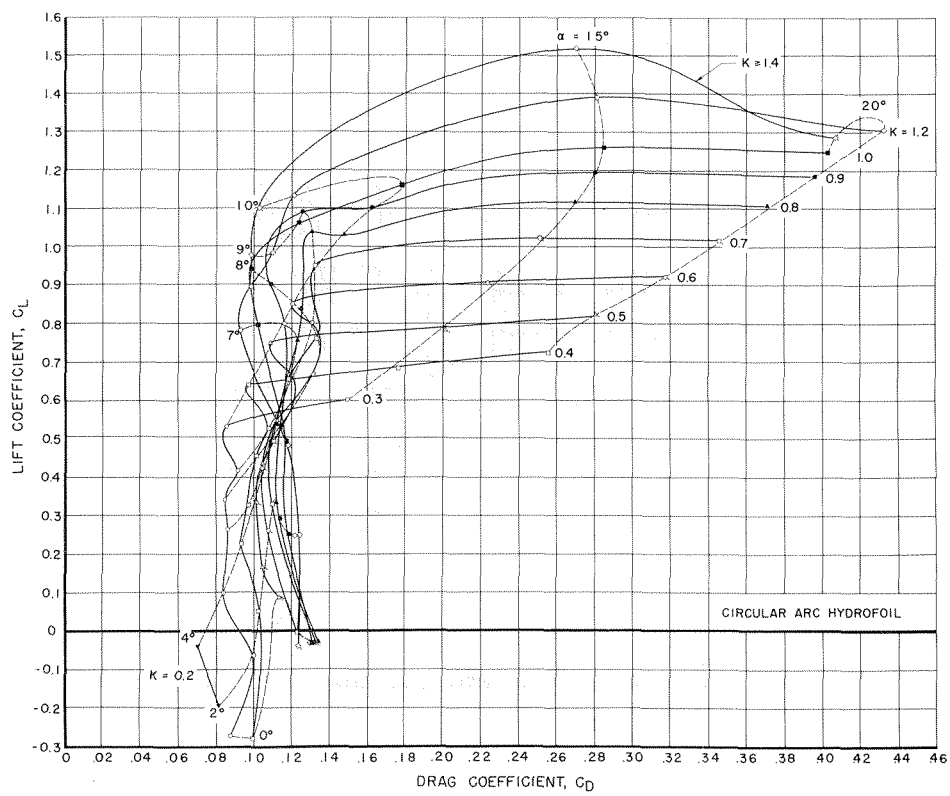

Fig. 23b - Cavitation polar diagram for the circular arc hydrofoil for the smaller values of α .

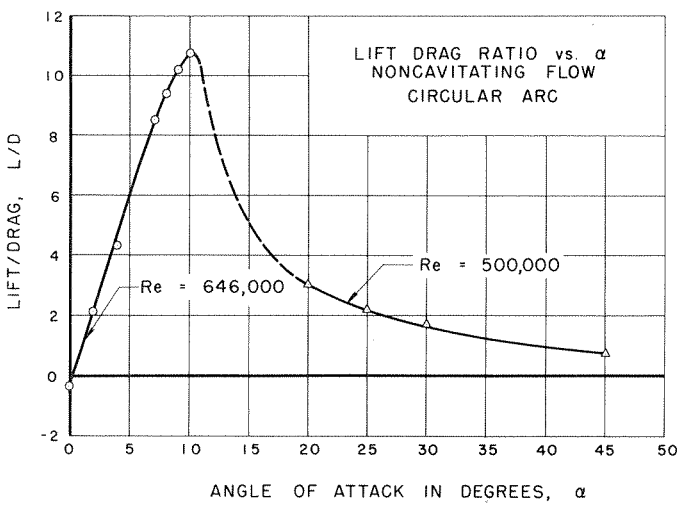

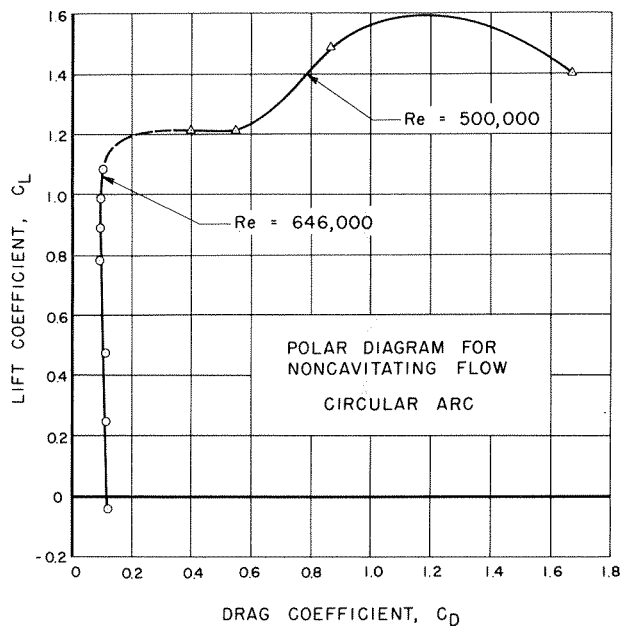

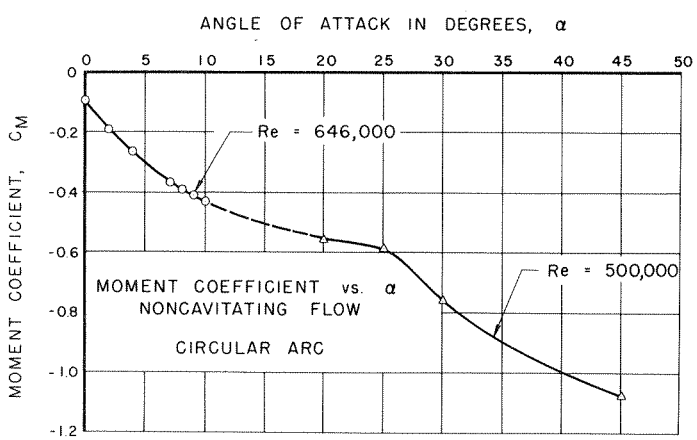

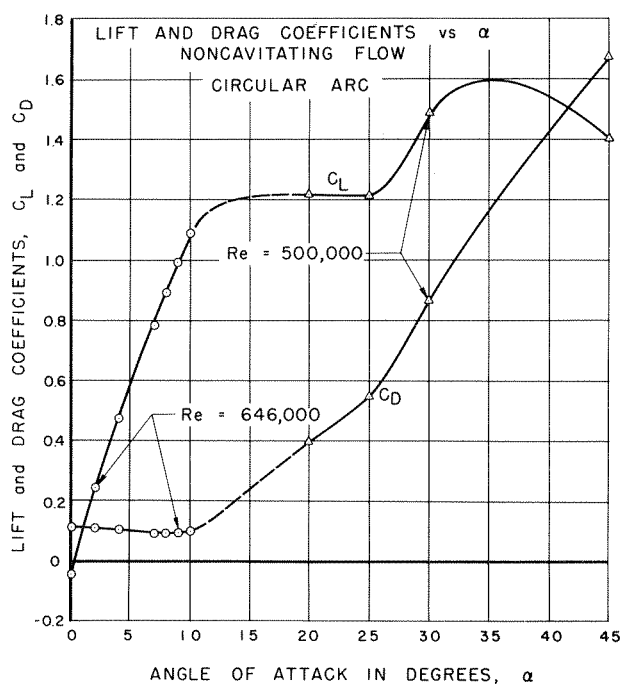

Fig. 24 - Hydrodynamic coefficients of the circular arc profile in noncavitating flow.

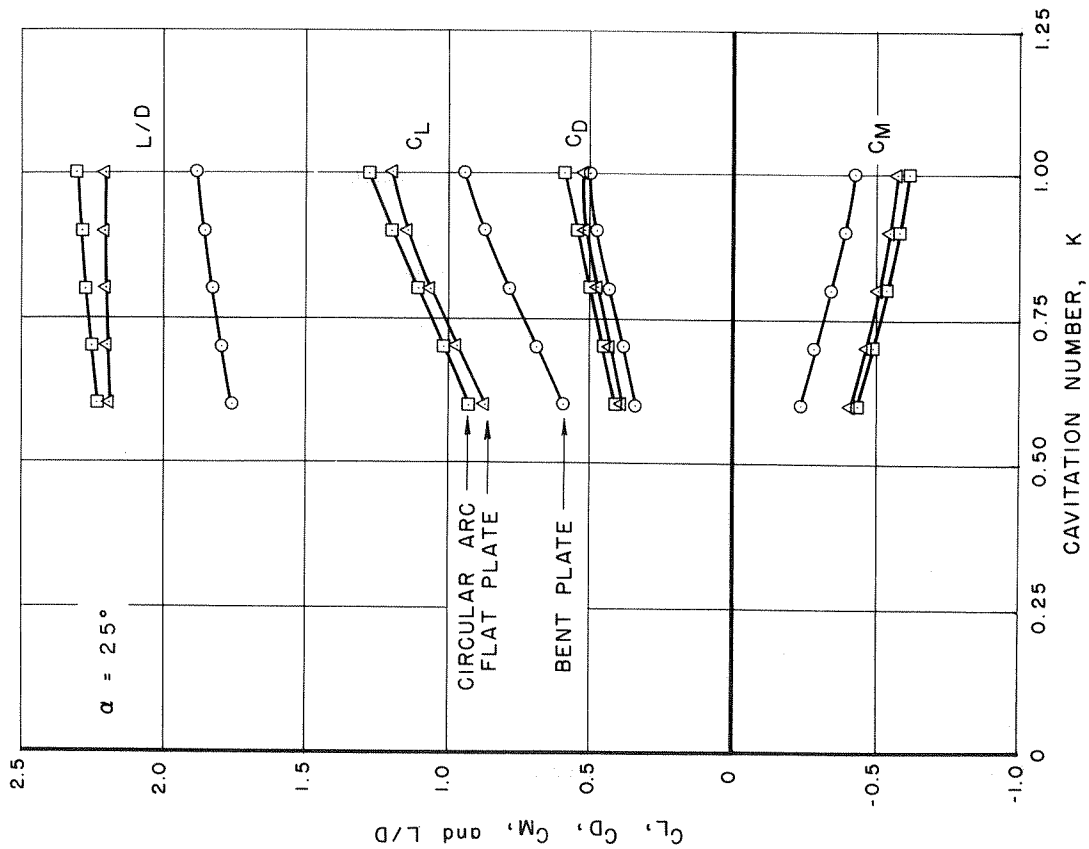

Fig. 25 - Experimental effects of camber at $\alpha = 25^{o}$.

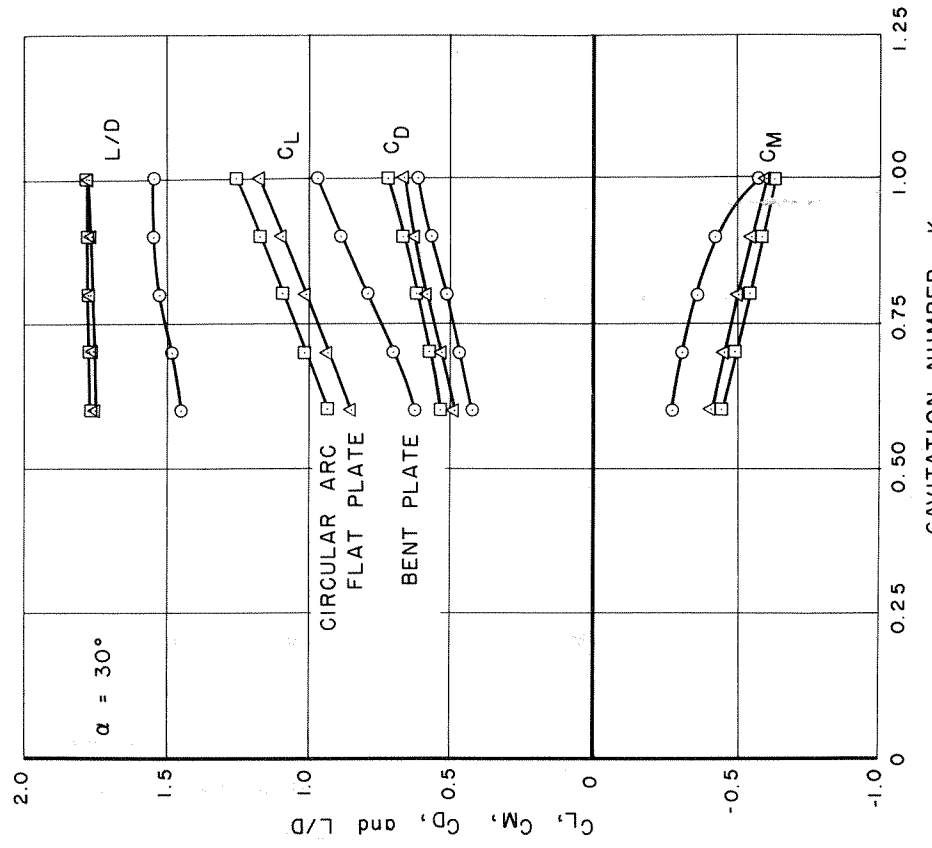

Fig. 26 - Experimental effects of camber at $\alpha = 30^{o}$.

SCALE EFFECTS

In the present experiments the major portion of the data was taken for partially or fully cavitating flows with the result that the cavitation number is the primary scaling parameter. Therefore we would expect nearly all of the present results to be directly applicable to practical use for larger hydrofoils. Of course, there may be pronounced Reynolds number effects for noncavitating flow past such sharp-edged profiles as were used in the present experiments. For this reason the Reynolds number at which the various data in noncavitating flow were taken is marked on the curves for each particular case in Figs. 18 and 24. In Fig. 24 the dotted line between the solid curves is intended to serve only as a guide to indicate a possible trend. For cavitation inception the first signs of cavitation appear in the wake vortex cores. It is known[7] that this phenomenon is very sensitive to Reynolds number. However, if one is not concerned with cavitation noise generation, such inception is of no importance because the forces on the profile appear to be unaffected by its occurrence.

COMPARISON WITH THEORY

As mentioned in the introduction, an important part of the present program is to provide an experimental check to Wu's theory for fully cavitating hydrofoils. The results of this exact theory for flat plate and circular arc profiles are presented in Ref. 1. In order to obtain a true comparison between experiment and theory we shall use those experimental results directly from the tables of data. We shall be very sparing in our use of cross-plotted coefficients. We shall concern ourselves mostly with comparisons between values of C_L, C_D and C_M because these are directly measured quantities.

In Figs. 27 through 29, flat plate experimental values of C_L, C_D and C_M are plotted against the cavitation number K for a wide range

of attack angles.* Theoretical curves from Wu's calculations are also given with the data. In the range of K and α where Wu's theory is fully applicable, the agreement is very good. Data points which are obviously outside the range of K and α for full cavity flows have been included in these plots to indicate the region within which the theory is valid. It can be seen that the agreement is generally best in the case of C_L and C_M for the lowest values of K and that deviations between theory and experiment appear to increase with increasing K. It also appears that the deviations in C_M are probably reflections of the deviations in C_L. They are generally consistent in sense with deviations in C_M which one would expect to result from the deviations observed in C_L. The agreement between the theoretical and experimental values for C_D appears to be well within the limits set by experimental scatter.

In Fig. 16 it was shown that the lift-drag ratio for the flat plate deviates from the cotangent rule and that this deviation takes the form of a tendency for the lift-drag ratio to increase with increasing cavitation numbers. On the other hand, Wu has found that his theory checks the cotangent rule for L/D. Evidently the experimentally observed trend of increasing L/D with K is due mainly to the deviations between the theoretical and measured values of C_L which, as noted above, show a dependence on the cavitation number. This dependence of the C_L deviations upon K at the lower attack angles is consistent with the observed trends of L/D with K.

The computed results from Ref. 1 are not as extensive in the case of the circular arc as they are for the flat plate. No curves of C_M vs K were calculated for this case and the computations made for C_L and C_D include $\alpha = 30^\circ$ as the highest attack angle considered. Figures 30 and 31 give a comparison of the appropriate experimental data with the available theoretical results for the circular arc profile. The agreement is good.

---

*For the flat plate data we have referred the attack angles to the lower surface of the wedge. For conciseness we have dropped the subscript c which we used previously to denote this angle. Moreover, in this section of the report, by K we mean K_k.

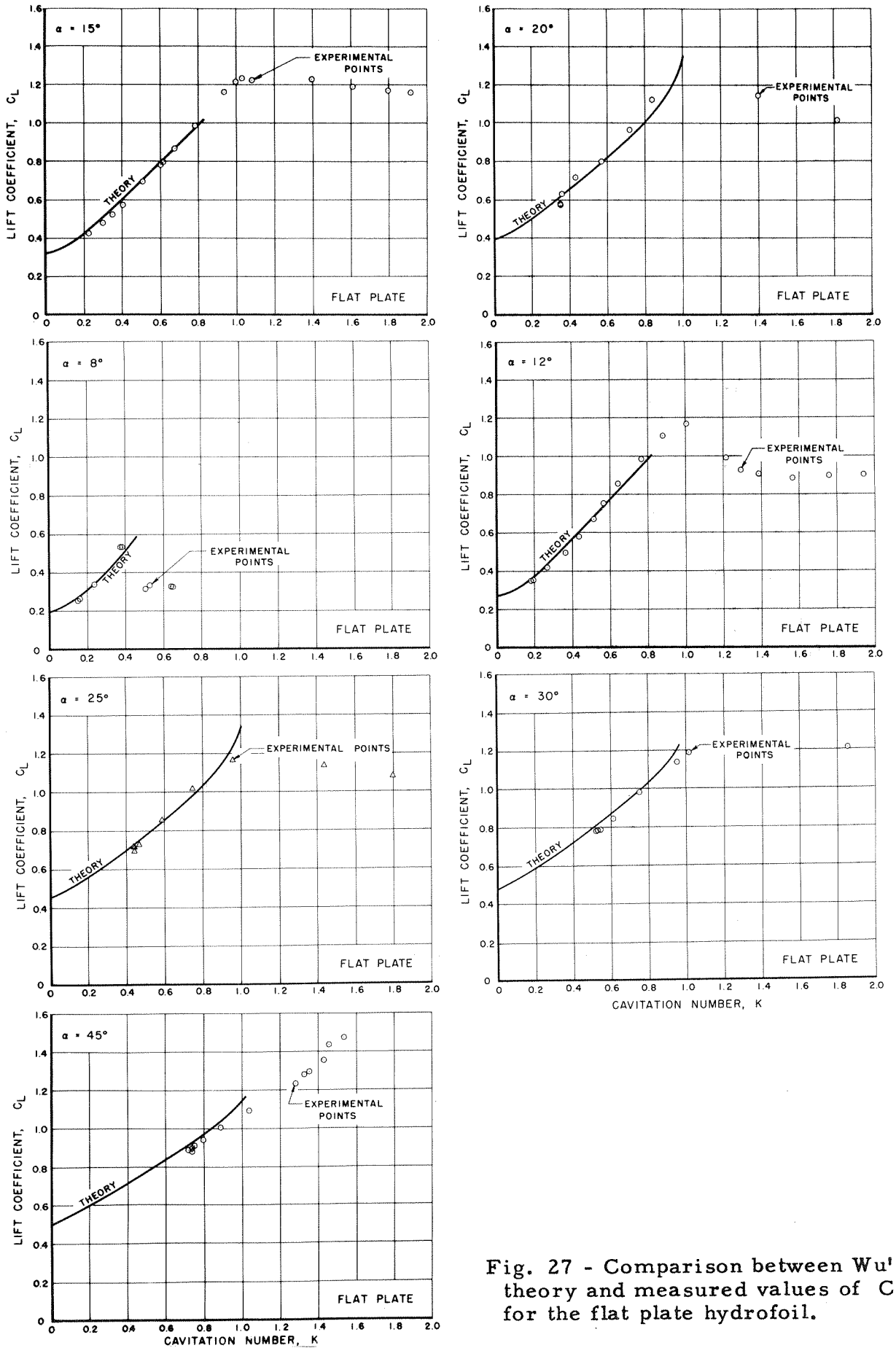

Fig. 27 - Comparison between Wu's theory and measured values of C_L for the flat plate hydrofoil.

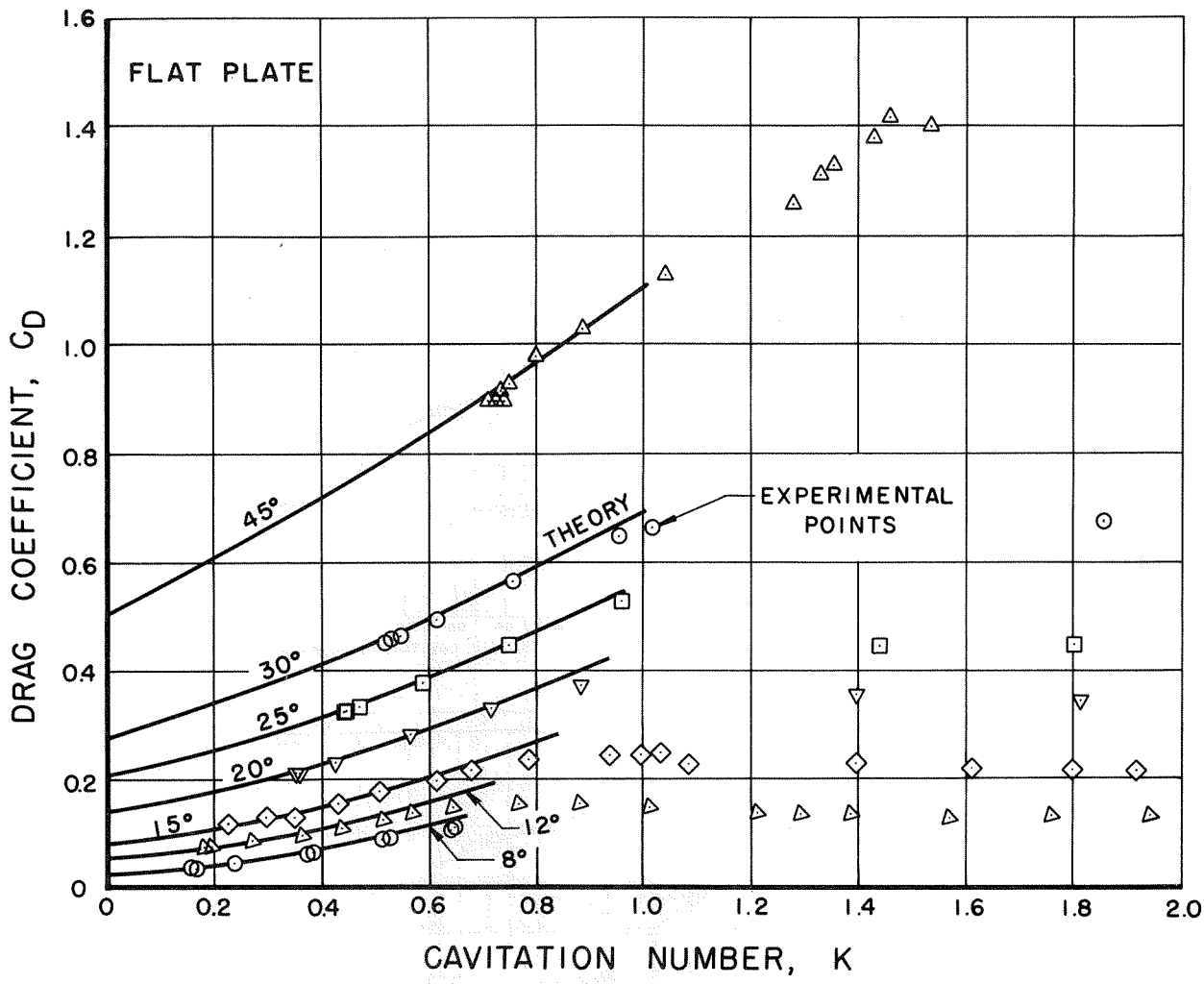

Fig. 28 - Comparison between Wu's theory and measured values of C_D for the flat plate hydrofoil.

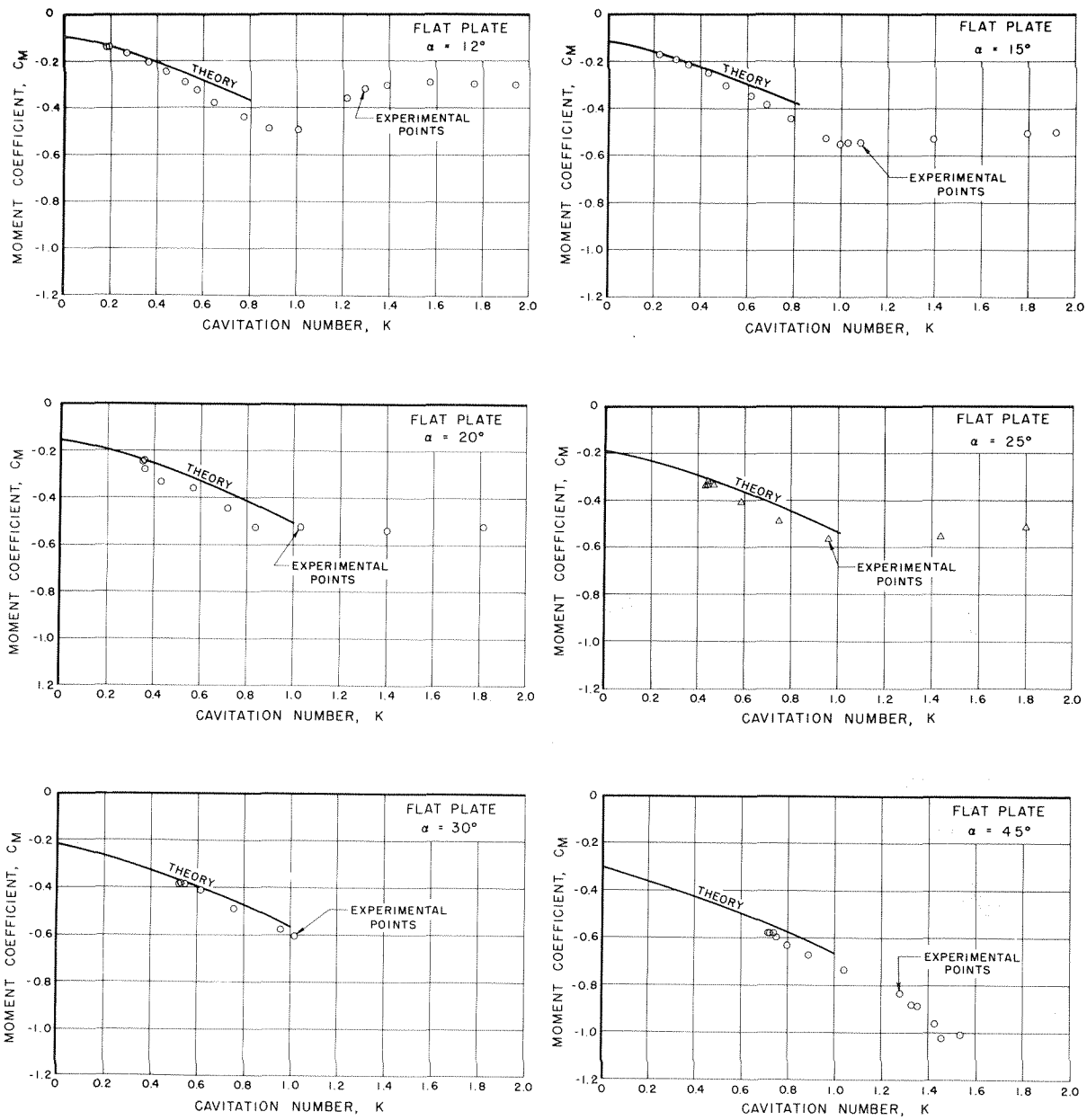

Fig. 29 - Comparison between Wu's theory and measured values of C_M for the flat plate hydrofoil.

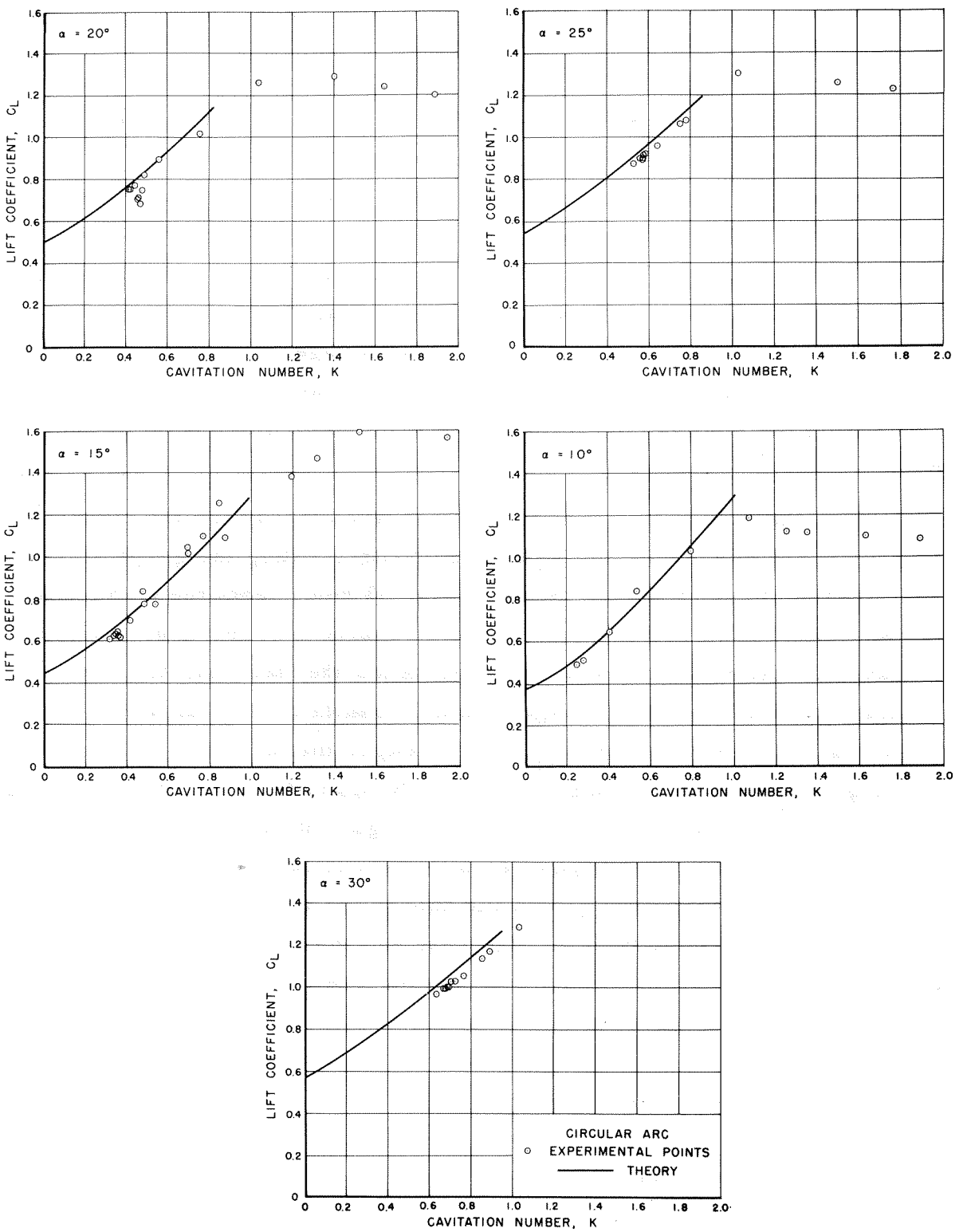

Fig. 30 - Comparison of Wu's theory and measured values of C_L for the circular arc hydrofoil.

The variety of flow configurations attainable with the circular arc model permits an interesting comparison between theory and experiment at low attack angles. Such a comparison is given in Fig. 32 where the experimental and the calculated results for C_L and C_D are compared. The theory requires the cavity to separate from the leading edge, while the experimental data result from a cavity flow which separates from the bend in the upper surface as shown. Of course, it is probably possible to design a circular arc profile for which the flow will correspond to the theoretical condition at these attack angles. Therefore we may regard Fig. 32 as a demonstration of the advantage to be gained in the present case by designing a sharp-edged profile so that the cavity will spring from the leading edge rather than from some other point on the upper surface.

When the values of C_L and C_D from Wu's theory for the circular arc profile are converted into values of lift-drag ratio, the graph of Fig. 22 results. The dashed curve of Fig. 33 represents the cotangent rule and is included with the circular arc results in order to give a comparison between the theoretical results for the flat plate and the circular arc profiles. If the experimental results of Fig. 22 are compared with Fig. 33 it can be seen that the experimental trend of increasing L/D with increasing K is directly opposite to the theoretically predicted trend. Moreover, we see from Figs. 30 and 31 that, as with the flat plate results, this opposition of trends is caused primarily by the deviations between experiment and theory for the lift component of force. We note that for both the flat plate and the circular arc profiles the experimental results usually indicate lift-drag ratios which are more favorable than those predicted by theory. For both profiles a tendency of L/D to increase with increasing K has been found experimentally. It also appears that the chief cause for this behavior rests with the lift rather than the drag. The cause for this behavior is not now understood, although we can conjecture that such an effect might possibly be caused by the influence of the tunnel walls, or perhaps a small consistent error has been unknowingly allowed to enter into the experiments. The problem of wall effects for symmetrical cavity flows where the only force is a drag force has already been investigated by Birkhoff, Plesset and

Simmons.[8] They found that, if the cavitation number is based on the cavity pressure, the drag coefficient for a given body is insensitive to the effects of the tunnel walls. Of course, this result is not directly applicable to the present situation. However, it is interesting to note that the experimentally determined drag coefficients for both shapes show excellent agreement with a theory in which the flow is of infinite extent. It is also noteworthy that whatever the cause of the present small deviations between experiment and theory, the effect appears to be limited solely to the lift force. A further investigation of these findings would be of interest.

A comparison between experimentally and theoretically determined camber effects is given in Fig. 34. The theoretical curves are taken from Wu's results for circular arc and flat plate profiles at $K = 0.6$ and $\alpha = 25^{\circ}$. The experimental points are taken from the data of Fig. 25. It is interesting to note that for the convex under-surface the calculated values of C_L and C_D for a convex circular arc profile are compared with experimental values taken from the flat plate. The comparison was made by requiring that for both the convex circular arc and the bent plate profiles, the flow should leave the sharp leading and trailing edges at the same angles. That is, the circular arc must be tangent to the lower surface of the bent plate at the leading and trailing edges. An arc for which $\gamma = 10^{\circ}5'$ closely meets this requirement. The good agreement between experiment and theory suggests that at the high attack angles for which this comparison was made, the angle at which the flow leaves the contour is of great importance, and that within the narrow limits considered here, the detailed nature of the contour between the separation points has little effect on the value of the force on the body.

CONCLUDING REMARKS

In the preceding sections experimental results for the forces and moments acting on two sharp-edged hydrofoils in cavitating and noncavitating flow have been presented. The influence of various flow configurations on the forces which act on a profile was found to be considerable.

The importance of correlating hydrofoil force data with the cavitation number based upon measured cavity pressure is also demonstrated. A comparison between experiment and Wu's nonlinearized theory of forces on profiles in full cavity flow showed good agreement. The small deviations which were found between the experimental and theoretical values of the lift suggest that further work be done to evaluate the influence of tunnel walls on fully cavitating hydrofoils.

ACKNOWLEDGMENT

It is a pleasure to acknowledge the participation of R. W. Kermeen, Z. M. Lindberg, R. L. Waid and T. Y. Wu in this experimental investigation. Their interest and assistance was of great value during the course of this work. Thanks are also due to Miss Donna Snyder for the illustrations and to Mrs. Rose Grant for preparing the manuscript.

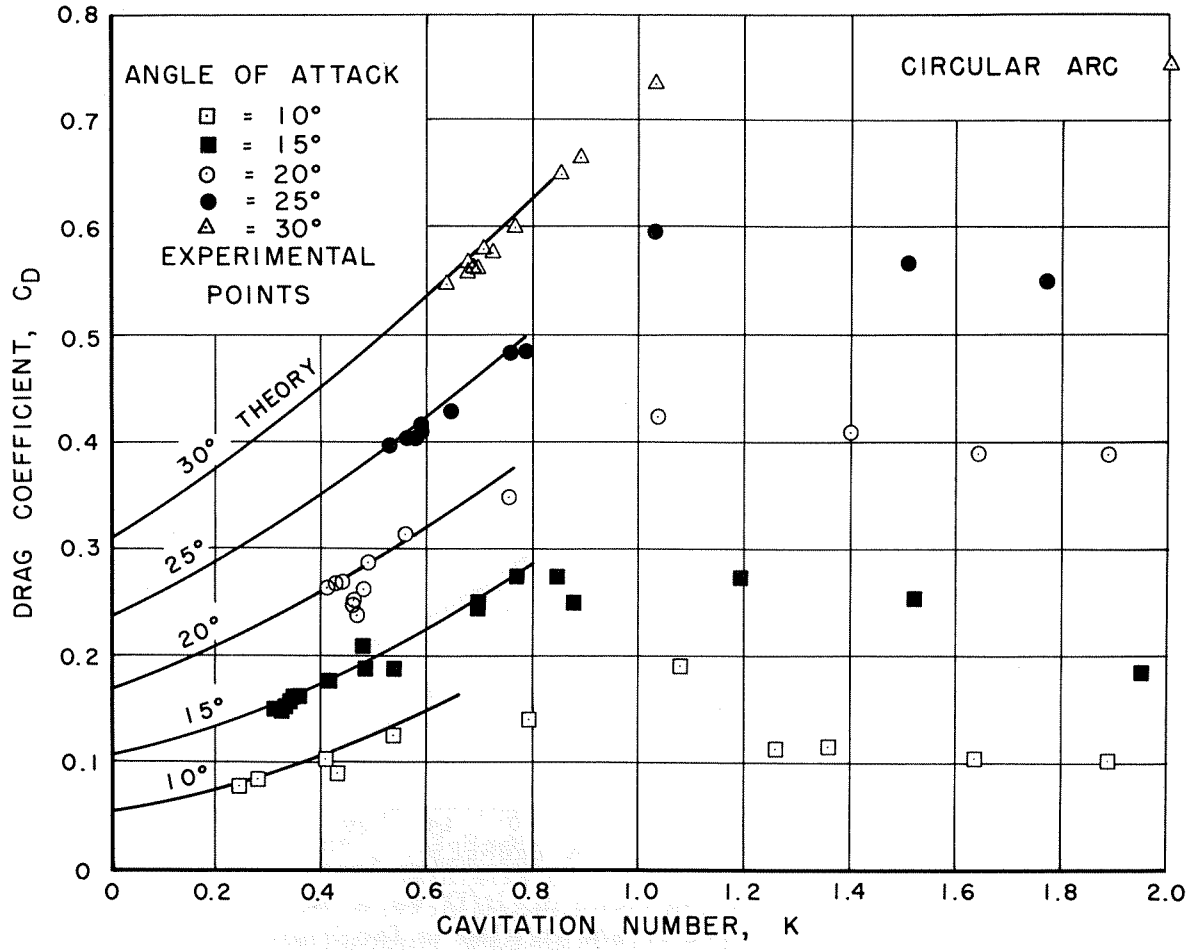

Fig. 31 - Comparison between Wu's theory and measured values of C_D for the circular arc hydrofoil.

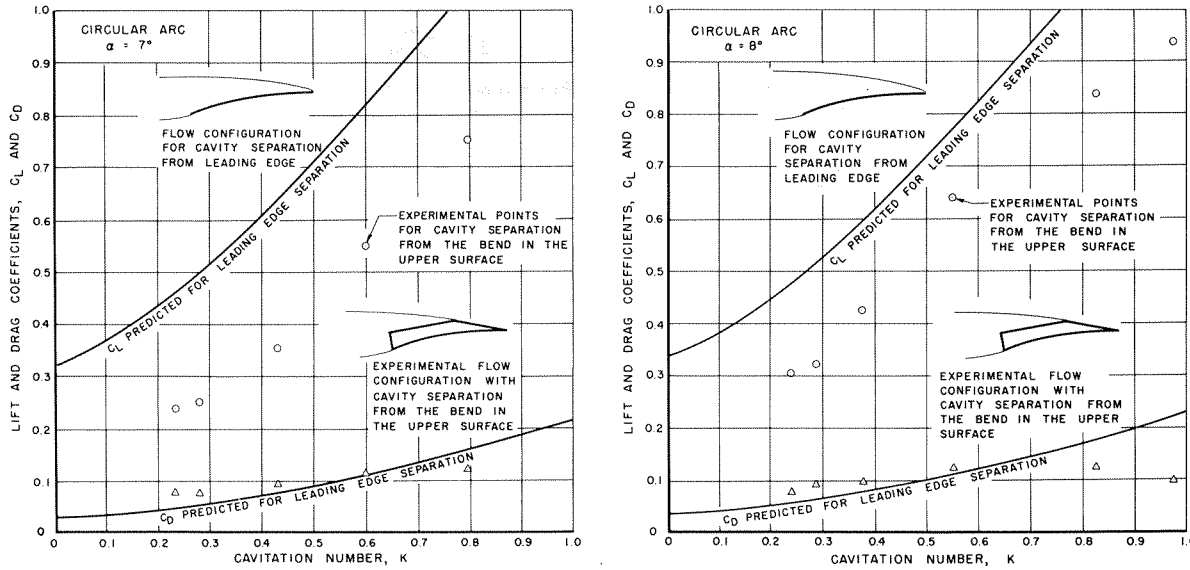

Fig. 32 - The solid lines show the values of C_L and C_D which would obtain for cavity detachment at the leading edge of the profile. The experimental points give values of C_L and C_D which result from the cavity detaching itself from the bend in the upper surface of the profile. These results show the effect of the cavity detachment position on the circular arc profile at two attack angles.

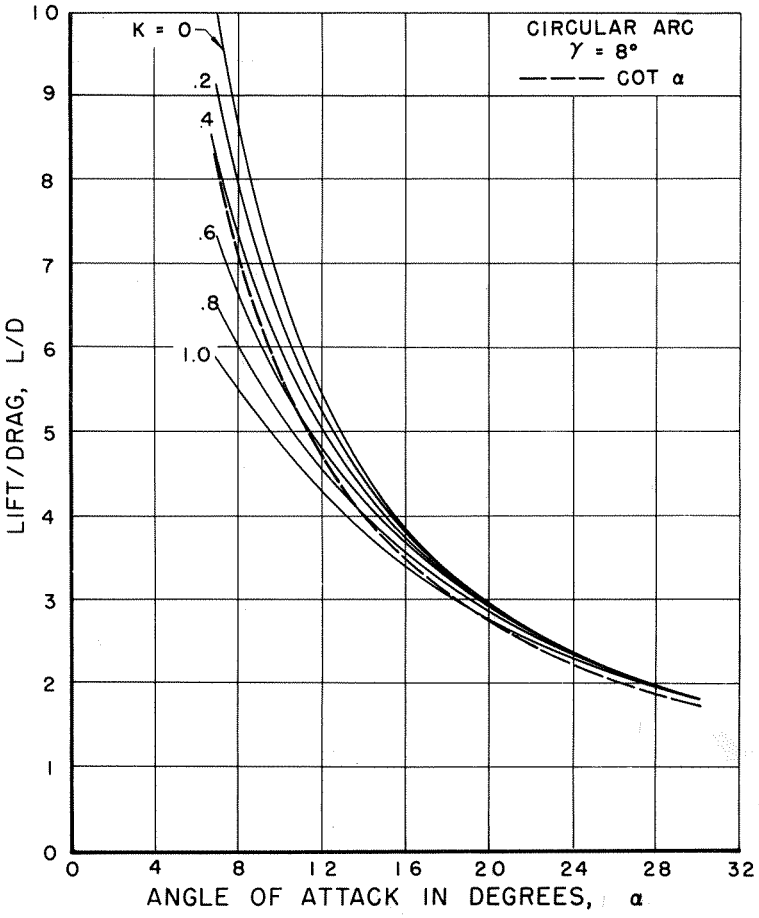

Fig. 33 - The theoretical trend in L/D vs α with K. The dashed cot α curve is shown also to facilitate the comparison of these curves with the experimental results summarized in Fig. 22.

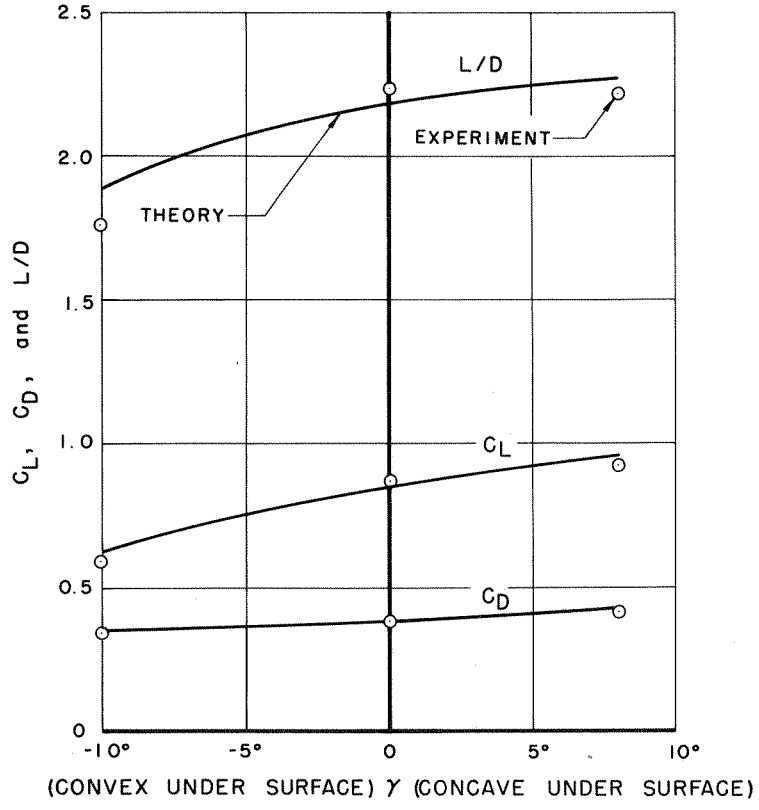

Fig. 34 - Comparison of theoretical and measured effects of camber at $\alpha = 25^{\circ}$.

REFERENCES

1. Wu, T. Yao-tsu, "A Free Streamline Theory for Two-Dimensional Fully Cavitated Hydrofoils", California Institute of Technology, Hydrodynamics Laboratory Report No. 21-17, July 1955.

2. Knapp, R.T., Levy, J., O'Neill, J.P. and Brown, F.B., "The Hydrodynamics Laboratory of the California Institute of Technology", Trans. ASME, Vol. 70, pp. 437-57, July 1948.

3. Kermeen, Robert W., "Water Tunnel Tests of NACA 4412 and Walchner Profile 7 Hydrofoils in Noncavitating and Cavitating Flows", California Institute of Technology, Hydrodynamics Laboratory Report No. 47-5, January 1956.

4. Hotz, G.M. and McGraw, J.T., "The High Speed Water Tunnel Three Component Force Balance", California Institute of Technology, Hydrodynamics Laboratory Report No. 47-2, December 1954.

5. Reichardt, H., "The Laws of Cavitation Bubbles at Axially Symmetrical Bodies in a Flow", Reports and Translations No. 776, Ministry of Aircraft Production, August 1946; distributed in U.S.A. by Office of Naval Research, Navy Department, Washington, D.C.

6. Roshko, Anatol, "On the Wake and Drag of Bluff Bodies", Journal of the Aeronautical Sciences, Vol. 22, No. 2, p. 124, February 1955.

7. Kermeen, McGraw and Parkin, "Mechanism of Cavitation Inception and the Related Scale Effects Problem", Trans. ASME, May 1955, p. 533.

8. Birkhoff, G., Plesset, M.S., and Simmons, N., "Wall Effects in Cavity Flow", Part I, Quarterly of Appl. Math., Vol. VIII, No. 2, p. 151, July 1950; Part II, Quarterly of Appl. Math., Vol. IX, No. 4, p. 413, January 1952.

TABLE I - FLAT PLATE OR WEDGE

Film No.	K_v	K_k	C_L	C_D	C_M	L/D
			$\alpha_c = 5^\circ$			
2	.608	.487*	.001	.0781	.004	.0128
3	.438	.360	.0012	.0589	.003	.0204
4	.265	.245	.002	.0404	.003	.0494
5	.175	.154	.001	.0304	.002	.0329
6	.155	.135	-.002	.0279	.002	-.0717
7	.141	.121	-.005	.0274	.004	-.1825
			$\alpha_c = 6^\circ$			
8	.826	.641*	.105	.0978	-.030	1.073
9	.636	.515*	.105	.0801	-.029	1.310
10	.455	.377	.100	.0615	-.026	1.625
11	.298	.266	.104	.0431	-.029	2.414
12	.210	.186	.101	.0363	-.024	2.882
13	.157	.140	.093	.0309	-.022	3.02
			$\alpha_c = 7^\circ$			
18	.239	.158*	.284	.0337	N.G.	8.43
19	.164	.145*	.231	.0255	N.G.	9.06
109	.803	.637*	.231	.179	-.078	1.29
110	.614	.504*	.226	.080	-.081	2.83
111	.450	.386	.225	.062	-.074	3.64
112	.255	.240	.319	.037	-.137	8.62
113	.166	.152	.247	.026	-.105	9.50
114	.145	.133	.231	.025	-.097	9.24
115	.142	.121	.228	.027	-.099	8.44
			$\alpha_c = 8^\circ$			
22	.804	.644*	.322	.1083		2.97
23	.622	.504*	.312	.0868		3.60
24	.436	.380	.532	.0632		8.42
25	.255	.235	.338	.0447	-.131	7.56
26	.178	.161	.264	.0372	-.096	7.10
27	.168	.154	.254	.0356	-.092	7.14
28	.804	.641*	.326	.1046	-.099	3.12
29	.633	.527*	.332	.0890	-.089	3.73
30	.444	.371	.533	.0639	-.213	8.34
			$\alpha_c = 9^\circ$			
31	.785	.630*	.466	.1110	-.137	4.19
32	1.006	.889*	.433	.1320	-.128	3.28
33	1.729	1.110*	.458	.1378	-.139	3.32
34	1.368	1.071*	.446	.1367	-.135	3.26
35	.593	.475*	.708	.0876	-.305	8.08
36	.428	.369*	.534	.0724	-.222	7.39
37	.280	.259	.373	.0561	-.145	6.65
38	.188	.173	.289	.0459	-.107	6.29
39	.174	.163	.286	.0437	-.106	6.54
			$\alpha_c = 10^\circ$			
40	1.729	.691	.584	.1215	-.179	4.81
41	1.376	.803	.576	.1273	-.174	4.52
42	1.192	.848	.566	.1393	-.170	4.06
43	1.007	.780	.570	.1323	-.177	4.31
44	.804	.618	.931	.1147	-.410	8.13
47	.598	.497	.731	.1037	-.316	7.05
48	.434	.379	.532	.0833	-.217	6.37
49	.255	.242	.363	.0598	-.138	6.07
50	.201	.185	.313	.0536	-.117	5.84
51	.198	.184	.310	.0524	-.115	5.92
			$\alpha_c = 11^\circ$			
52	1.761		.746	.1217	-.239	6.13
53	1.405		.749	.1242	-.233	6.03
54	1.005		1.103	.1325	-.478	8.33
55	.808		.948	.1363	-.414	6.95
56	.616	.521*	.741	.1253	-.316	5.91
57	.443	.391	.533	.0999	-.212	5.34
58	.257	.234	.384	.0674	-.141	5.70
59	.216	.203	.343	.0650	-.118	5.28
60	.209	.195	.343	.0666	-.128	5.15

Film No.	K_v	K_k	C_L	C_D	C_M	L/D
			$\alpha_c = 12^\circ$			
2a	4.285		.899	.1312	-.307	6.84
3a	2.646		.915	.1313	-.313	6.96
4a	2.217		.896	.1306	-.302	6.82
5a	1.940		.900	.1314	-.303	6.84
6a	1.758		.896	.1313	-.298	6.82
7a	1.567		.882	.1293	-.292	6.82
8a	1.384		.905	.1327	-.305	6.82
9a	1.292		.924	.1349	-.318	6.84
10a	1.213		.990	.1384	-.359	7.16
11a	1.123	1.006*	1.171	.1467	-.492	5.22
12a	.968	.880*	1.108	.1534	-.487	4.32
13a	.833	.769	.985	.1546	-.437	6.37
14a	.705	.643	.856	.1487	-.375	5.76
15a	.624	.566	.754	.1384	-.324	5.45
16a	.534	.513	.673	.1263	-.287	5.33
17a	.452	.434	.583	.1116	-.244	5.23
18a	.377	.362	.498	.0989	-.202	5.04
19a	.284	.268	.421	.0863	-.165	4.88
20a	.208	.193	.355	.0764	-.136	4.65
21a	.191	.180	.351	.0747	-.137	4.70
22a	2.687		.919	.1302	-.319	7.06
			$\alpha_c = 13^\circ$			
24a	4.329		1.076	.1585	-.406	6.78
25a	2.665		1.097	.1607	-.419	6.82
26a	2.207		1.055	.1602	-.397	6.58
27a	1.949		1.073	.1599	-.403	6.72
28a	1.749		1.072	.1593	-.400	6.73
29a	1.580	1.052*	1.072	.1597	-.398	6.72
30a	1.383	1.094*	1.140	.1640	-.450	6.95
31a	1.241	1.065*	1.160	.1642	-.479	7.06
32a	1.175	1.060	1.218	.1785	-.527	6.82
33a	1.096	1.003	1.207	.1869	-.538	6.46
34a	.962	.894	1.118	.1846	-.505	6.06
35a	.843	.790	.987	.1857	-.447	5.32
36a	.732	.684	.880	.1762	-.398	4.99
38a	.677	.646	.805	.1666	-.360	4.83
39a	.550	.523	.688	.1472	-.291	4.67
40a	.451	.429	.584	.1280	-.253	4.56
41a	.346	.329	.497	.1134	-.216	4.38
42a	.256	.239	.429	.0991	-.181	4.33
43a	.218	.202	.377	.0901	-.157	4.18
44a	.204	.188	.373	.0876	-.157	4.26
45a	2.665		1.062	.1559	-.410	6.82
			$\alpha_c = 15^\circ$			
69a	4.445		1.155	.2175	-.502	5.32
70a	2.684		1.156	.2159	-.502	5.35
71a	2.241		1.167	.2156	-.504	5.42
72a	1.914		1.158	.2146	-.500	5.38
73a	1.794		1.169	.2140	-.504	5.46
74a	1.607		1.189	.2176	-.508	5.47
75a	1.394	1.069*	1.227	.2265	-.532	5.41
76a	1.277	1.081*	1.223	.2289	-.544	5.34
77a	1.174	1.030*	1.232	.2459	-.543	5.02
78a	1.118	.994	1.214	.2438	-.552	4.98
79a	1.037	.935	1.161	.2435	-.528	4.77
80a	.852	.783	.988	.2332	-.446	4.23
81a	.730	.679	.868	.2142	-.385	4.04
82a	.651	.613	.797	.1992	-.348	4.00
83a	.538	.506	.696	.1790	-.301	3.89
84a	.453	.430	.591	.1553	-.250	3.80
85a	.366	.349	.523	.1397	-.218	3.77
86a	.308	.294	.480	.1290	-.196	3.72
87a	.235	.223	.425	.1189	-.172	3.58
90a	2.752		1.175	.2209	-.514	5.32
63	2.647			.2236		
64	1.736			.2269		
65	1.383	.545*		.2366		
66	.984	.720*		.2488		
67	.830	.714*		.2294		
68	.641	.564		.1918		
69	.451	.417		.1522		
70	.298	.287		.1217		
71	.282	.273		.1215		
72	.334	.279		.1263		

* For these runs the measured difference between the barometric pressure and the cavity pressure was less than 2.31 ft of mercury. This condition corresponded to flows with the relatively short foamy cavities of the higher cavitation numbers where accurate cavity pressure readings were hard to obtain.

TABLE I - Continued

Film No.	K_v	K_k	C_L	C_D	C_M	L/D
			$\alpha_c = 17^\circ$			
92a	4.507		1.062	.2731	-.484	3.89
93a	2.750		1.061	.2733	-.484	3.89
94a	2.250		1.115	.2807	-.508	3.97
95a	1.950		1.098	.2776	-.501	3.96
96a	1.735		1.061	.2710	-.485	3.92
97a	1.640		1.119	.2802	-.511	3.99
98a	1.414	.968*	1.163	.2860	-.530	4.07
99a	1.318	1.036*	1.223	.3043	-.566	4.02
100a	1.225	1.019*	1.219	.3099	-.569	3.94
101a	1.120	.955	1.167	.3047	-.537	3.83
102a	1.066	.956	1.134	.3032	-.519	3.74
103a	.931	.841	1.050	.2958	-.478	3.55
104a	.839	.752	.960	.2813	-.430	3.42
105a	.752	.699	.876	.2613	-.389	3.35
106a	.630	.585	.770	.2364	-.335	3.26
107a	.542	.512	.697	.2161	-.301	3.22
108a	.421	.397	.586	.1866	-.246	3.14
109a	.375	.358	.550	.1751	-.230	3.14
110a	.287	.271	.485	.1574	-.197	3.08
111a	.272	.261	.476	.1547	-.191	3.08
112a	.269	.257	.477	.1559	-.195	3.06
113a	4.331		1.065	.2773	-.490	3.84
			$\alpha_c = 20^\circ$			
73	2.752		1.035	.3464	-.487	2.98
74	1.813		1.092	.3420	-.519	3.19
75	1.397		1.143	.355	-.540	3.22
76	1.028	.833*	1.123	.371	-.525	3.03
77	.833	.715*	.965	.332	-.444	2.91
78	.650	.564*	.801	.282	-.359	2.84
79	.458	.428	.721	.232	-.332	3.11
80	.364	.356	.633	.213	-.282	2.97
81	.361	.353	.574	.212	-.244	2.71
82	.357	.349	.580	.211	-.248	2.75
			$\alpha_c = 25^\circ$			
83	2.752		1.113	.487	-.546	2.28
84	1.798		1.078	.446	-.515	2.42
85	1.438		1.133	.487	-.554	2.32
86	1.147	.958*	1.161	.528	-.565	2.20
87	.854	.747*	1.014	.445	-.488	2.28
88	.632	.584	.854	.377	-.408	2.26
89	.486	.469	.723	.333	-.336	2.17
90	.456	.441	.691	.325	-.318	2.13
91	.451	.442	.707	.324	-.329	2.18
92	.444	.434	.713	.321	-.336	2.22
			$\alpha_c = 30^\circ$			
93	2.815		1.235	.676	-.628	1.83
94	1.853		1.213	.674	-.623	1.80
95	1.486	1.016*	1.189	.663	-.606	1.80
96	1.109	.955*	1.144	.647	-.528	1.77
97	.853	.752*	.987	.563	-.491	1.74
98	.649	.612	.850	.493	-.412	1.73
99	.559	.544	.794	.461	-.387	1.72
100	.543	.525	.787	.457	-.382	1.72
101	.539	.519	.784	.451	-.385	1.74
			$\alpha_c = 45^\circ$			
115a	6.389		1.561	1.458	-1.085	1.071
116a	6.219		1.512	1.455	-1.052	1.040
117a	6.023		1.562	1.444	-1.079	1.081
118a	5.768		1.529	1.446	-1.060	1.058
119a	5.576		1.544	1.446	-1.060	1.061
120a	5.359		1.520	1.451	-1.054	1.048
121a	5.146		1.496	1.433	-1.040	1.042
122a	4.924		1.470	1.438	-1.021	1.022
123a	4.743		1.508	1.438	-1.053	1.049
124a	4.522		1.518	1.457	-1.057	1.042
125a	4.230		1.506	1.427	-1.028	1.056
126a	3.994		1.545	1.432	-1.054	1.078
127a	3.717		1.538	1.430	-1.053	1.075
128a	3.461		1.515	1.437	-1.047	1.054
129a	3.231		1.585	1.443	-1.087	1.098
130a	2.948		1.522	1.443	-1.049	1.055
131a	2.634	1.535*	1.474	1.400	-1.010	1.053
132a	2.361	1.457*	1.437	1.416	-1.021	1.016
133a	2.059	1.429*	1.353	1.379	-.961	.975
			$\alpha_c = 45^\circ$ - continued			
134a	1.777	1.351	1.297	1.325	-.886	.978
135a	1.679	1.328	1.284	1.310	-.878	.981
136a	1.532	1.279	1.234	1.255	-.833	.983
137a	1.183	1.038	1.095	1.124	-.735	.974
138a	1.007	.886	1.009	1.026	-.670	.983
139a	.881	.797	.946	.977	-.630	.968
140a	.812	.748	.913	.927	-.595	.984
141a	.791	.738	.902	.914	-.587	.988
142a	.767	.720	.891	.901	-.578	.989
143a	.757	.714	.896	.900	-.581	.996
144a	.740		.886	.894	-.577	.991
145a	4.102		1.447	1.406	-.997	1.028
146a	6.477		1.569	1.431	-1.063	1.093
147a	8.610		1.567	1.431	-1.067	1.092
			$\alpha_c = 60^\circ$			
105	1.993	1.803*	1.182	2.005	-1.104	.589
106	1.262	1.139*	.912	1.570	-.843	.580
107	1.310	1.218	.941	1.623	-.869	.580
108	1.071	.988	.836	1.458	-.774	.573

TABLE II - CIRCULAR ARC

Film No.	K_v	K_k	C_L	C_D	C_M	L/D
			$\alpha = 0^\circ$			
123	2.667		-.0410	.1171	-.0953	-.35
124	1.398		-.0349	.1210	-.0958	-.29
125	1.018		-.0247	.1253	-.1025	-.197
126	.834	.621*	-.0116	.1314	-.1147	-.088
127	.651	.529*	+.0775	.1112	-.1866	+.698
128	.421	.391	-.3077	.0968	+.0688	-3.18
129	.273		-.2548	.0844	+.0566	-3.02
131	.615	.457*	+.0551	.1125	-.1692	+.49
132	.414	.346*	-.3065	.0950	+.0680	-3.23
133	.277	.259	-.2529	.0833	+.0540	-3.03
			$\alpha = 2^\circ$			
134	2.568		+.2478	.1132	-.1906	+2.19
135	1.358		.2547	.1308	-.1921	1.95
136	.985		.2579	.1163	-.1986	2.31
137	.714		.3379	.1002	-.2705	3.38
138	.421	.335*	-.0226	.1001	-.1077	-.226
139	.270	.161*	-.2372	.0699	+.0495	-3.39
			$\alpha = 4^\circ$			
140	2.548		+.4775	.1097	-.2659	+4.36
141	1.154		.4883	.1125	-.2729	4.34
142	.815		.5431	.0977	-.3389	5.55
143	.607	.490*	.3193	.1026	-.2336	3.11
144	.436	.370*	.1597	.0906	-.1541	1.76
145	.264	.246	.0089	.0753	-.0882	0.118
146	.234	.219	-.0182	.0709	-.0802	-.256
			$\alpha = 7^\circ$			
147	2.492		.7786	.0929	-.3562	8.38
148	2.529		.7835	.0917	-.3647	8.54
149	1.588		.7917	.0958	-.3626	8.26
150	1.296		.7917	.0954	-.3649	8.30
151	1.142		.7825	.0896	-.3640	8.73
152	.795		.7525	.1211	-.3881	6.22
153	.598		.5486	.1141	-.2931	4.81
154	.429		.3546	.0936	-.2042	3.79
155	.278		.2493	.0764	-.1537	3.27
156	.257	.231	.2384	.0767	-.1494	3.11
			$\alpha = 8^\circ$			
157	2.529		.8932	.0952	-.3899	9.38
158	1.826		.8907	.0946	-.3894	9.41
159	1.616		.9009	.0993	-.3939	9.07
160	1.352		.8797	.0976	-.3861	9.01
161	.974		.9392	.0992	-.4310	9.47
162	.825		.8399	.1234	-.4090	6.80
163	.642	.549*	.641	.1243	-.3200	5.16
164	.414	.375	.427	.0978	-.2233	4.37
165	.277	.285	.322	.0815	-.1747	3.95
166	.253	.237	.306	.0780	-.1686	3.92

TABLE II - Continued

Film No.	K_v	K_k	C_L	C_D	C_M	L/D
			$\alpha = 9^\circ$			
167	2.627		.991	.0974	-.4106	10.17
168	1.706		.979	.0982	-.4075	9.96
169	1.339		.996	.0997	-.4151	10.00
170	1.075		1.021	.1016	-.4312	10.02
171	.855		1.089	.1170	-.4927	9.30
172	.786		1.028	.1218	-.4646	8.44
173	.607	.523*	.698	.1244	-.3291	5.61
174	.429	.385	.513	.1048	-.2465	4.90
175	.298	.284	.396	.0868	-.1937	4.56
176	.264	.246	.376	.0838	-.1848	4.48
			$\alpha = 10^\circ$			
177	2.587		1.089	.1012	-.4317	10.75
178	1.886		1.081	.1031	-.4314	10.49
179	1.630		1.099	.1039	-.4389	10.58
180	1.358		1.113	.1153	-.4463	9.66
182	1.255		1.121	.1125	-.4416	9.97
183	1.075		1.186	.1904	-.4930	9.95
184	.792		1.026	.1402	-.4627	7.32
185	.615	.535*	.840	.1271	-.3750	6.61
186	.444	.405	.647	.1049	-.2858	6.17
187	.295	.279	.511	.0845	-.2248	6.05
188	.264	.246	.493	.0809	-.2170	6.10
			$\alpha = 15^\circ$			
191	.904	.767*	1.100	.275	-.4920	4.01
192	.803	.693*	1.019	.250	-.4531	4.07
193	.615	.475	.834	.211	-.3660	3.95
194	.443	.414	.699	.177	-.3048	3.95
195	.377	.355	.643	.164	-.2788	3.92
196	.366	.345	.636	.162	-.2760	3.93
266	1.072	.842*	1.256	.275	-.5641	4.57
267	1.317		1.465	.288	-.6504	5.08
268	.824	.692*	1.046	.245	-.4655	4.27
269	.665	.483	.774	.190	-.3362	4.08
270	.358	.333	.629	.156	-.2723	4.03
271	.344	.313	.613	.152	-.2625	4.03
272	5.515		1.436	.177	-.5305	8.11
273	3.160		1.466	.177	-.5354	8.29
274	2.616		1.481	.177	-.5343	8.36
275	2.249		1.494	.181	-.5448	8.26
276	1.948		1.566	.184	-.5912	8.51
277	1.520		1.592	.255	-.6804	6.24
278	1.192		1.381	.273	-.6157	5.06
279	.872		1.092	.251	-.4893	4.35
280	.536		.774	.189	-.3395	4.09
281	.358	.334	.621	.154	-.2686	4.03
282	.367	.328	.618	.152	-.2674	4.07
			$\alpha = 20^\circ$			
198	.843	.752*	1.018	.350	-.4623	2.91
199	.606	.555	.896	.314	-.4027	2.85
200	.506	.479	.750	.262	-.3332	2.86
201	.485	.467	.686	.239	-.3045	2.87
202	.482	.459	.717	.251	-.3183	2.86
203	.474	.455	.708	.247	-.3138	2.87
262	.460	.424	.749	.266	-.3393	2.82
263	.457	.418	.747	.263	-.3369	2.84
253	4.312		1.218	.399	-.5561	3.05
254	2.456		1.218	.401	-.5482	3.04
255	1.884		1.201	.390	-.5460	3.08
256	1.640		1.234	.388	-.5563	3.18
257	1.400		1.284	.407	-.5849	3.15
258	1.106	1.034	1.259	.423	-.5794	2.97
260	.547	.488	.820	.288	-.3693	2.85
261	.467	.440	.771	.271	-.3463	2.84
			$\alpha = 25^\circ$			
205	.874	.782*	1.078	.486	-.5081	2.22
206	.687	.646	.953	.429	-.4450	2.22
207	.597	.587	.915	.411	-.4252	2.226
207a	.608	.574	.901	.406	-.4173	2.22
208	.603	.576	.897	.406	-.4153	2.21
243	4.540		1.213	.547	-.5873	2.22
244	2.773		1.244	.565	-.6001	2.20
245	2.031		1.216	.553	-.5896	2.20
246	1.768		1.219	.550	-.5911	2.22
247	1.505		1.251	.567	-.6054	2.21
248	1.270	1.030*	1.300	.595	-.6268	2.19
249	.853	.755*	1.062	.483	-.5046	2.20
250	.632	.583	.921	.417	-.4320	2.20
251	.588	.559	.892	.405	-.3825	2.20
252	.556	.528	.870	.398	-.4074	2.18

Film No.	K_v	K_k	C_L	C_D	C_M	L/D
			$\alpha = 30^\circ$			
210	1.010	.889	1.165	.663	-.5778	1.76
211	.814	.764	1.052	.598	-.5181	1.76
212	.767	.724	1.027	.577	-.5018	1.75
213	.728	.694	.999	.563	-.4874	1.774
214	.719	.685	.998	.561	-.4875	1.78
215	.708	.673	.988	.555	-.4794	1.80
235	5.738		1.489	.866	-.7599	1.718
236	2.633		1.324	.773	-.6385	1.808
237	2.006		1.308	.750	-.6609	1.745
238	1.373	1.030*	1.282	.734	-.6477	1.748
239	.963	.853*	1.136	.648	-.5687	1.752
240	.768	.703	1.025	.578	-.5079	1.775
241	.713	.669	.996	.562	-.4932	1.770
242	.678	.634	.967	.548	-.4668	1.764
			$\alpha = 45^\circ$			
216	2.021	1.747*	1.494	1.536	-.9695	0.974
217	1.354	1.215*	1.257	1.244	-.7844	1.010
218	1.176	1.084	1.176	1.174	-.7300	1.009
219	1.110	1.035	1.151	1.148	-.7118	1.004
220	.919	.839	1.137	1.132	-.7057	1.004
228	1.934	1.651*	1.455	1.498	-.9468	.972
229	1.199	1.086	1.301	1.314	-.8303	.992
230	1.095	1.005	1.151	1.145	-.7211	1.004
231	1.041	.963	1.133	1.125	-.7116	1.007
232	1.044	.959	1.132	1.121	-.7012	1.011
233	4.240		1.426	1.708	-.9957	.835
234	7.803		1.402	1.670	-.9765	.835
			$\alpha = 60^\circ$			
221	1.339	1.219	.979	1.701	-.9010	.575
222	1.405	1.317	1.001	1.737	-.9224	.582
223	1.518	1.377	1.025	1.804	-.9448	.567
224	2.337	2.175*	1.254	2.265	-1.2082	.553
225	2.936		1.246	2.443	-1.2744	.508

TABLE III - BENT PLATE

Film No.	K_v	K_k	C_L	C_D	C_M	L/D
			$\alpha = 23^\circ 40'$			
283	1.286		.970	.468	-.437	2.08
284	1.059	.900*	.886	.444	-.388	2.00
285	0.810	.706*	.687	.365	-.280	1.86
286	0.629	.559*	.557	.309	-.213	1.80
			$\alpha = 25^\circ 40'$			
287	1.312		.932	.498	-.437	1.87
288	1.106	.969*	.925	.512	-.419	1.81
289	.851	.742*	.735	.418	-.319	1.76
290	.629	.591	.594	.349	-.242	1.72
			$\alpha = 29^\circ 40'$			
291	1.324	.985*	.963	.607	-.467	1.586
292	1.338	1.014*	.966	.614	-.470	1.575
293	.926	.822*	.799	.525	-.368	1.540
294	.703	.659	.669	.450	-.297	1.485
295	.650	.615	.635	.433	-.279	1.466
296	.627	.602	.623	.416	-.273	1.467
297	.606	.583	.618	.412	-.270	1.471
298	.576	.545	.598	.400	-.265	1.468
			$\alpha = 39^\circ 40'$			
299	1.721		1.152	1.061	-.701	1.084
300	2.025		1.219	1.128	-.749	1.082
301	1.724		1.160	1.068	-.696	1.086
302	1.001	.923	.867	.798	-.496	1.086
303	.887	.829	.813	.748	-.458	1.086
304	.847	.776	.804	.734	-.454	1.096
305	.832	.774	.800	.718	-.451	1.097
			$\alpha = 54^\circ 40'$			
306	2.053		1.172	1.733	-.985	.686
307	1.280	1.181	.900	1.338	-.740	.673
308	1.239	1.157	.886	1.323	-.728	.670
309	1.168	1.093	.864	1.282	-.710	.673
			$\alpha = 69^\circ 40'$			
310	2.562	2.262*	.886	2.460	-1.321	.371
311	1.597	1.466	.692	1.907	-.992	.372
312	1.540	1.425	.682	1.860	-.970	.367
313	1.474	1.391	.673	1.823	-.953	.369

DISTRIBUTION LIST FOR TECHNICAL REPORTS ISSUED UNDER CONTRACT NONR-220(12)

Item	Address	No. Copies
1	Commanding Officer and Director, David Taylor Model Basin, Washington 7, D.C., Attn: Code 580	54
2	Chief of Naval Research, Office of Naval Research, Department of the Navy, Washington 25, D.C., Attn: Mechanics Branch (Code 438)	6
3	Commanding Officer, Branch Office, Office of Naval Research, 495 Summer St., Boston 10, Mass.	1
4	Commanding Officer, Branch Office, Office of Naval Research, 346 Broadway, New York 13, N. Y.	1
5	Commanding Officer, Branch Office, Office of Naval Research, The John Crerar Library Bldg., 10th Floor, 86 E. Randolph St., Chicago 1, Ill.	1
6	Commanding Officer, Bran ch Office, Office of Naval Research, 1000 Geary St., San Francisco 9, Calif.	1
7	Commanding Officer, Branch Office, Office of Naval Research, 1030 E. Green Street, Pasadena 1, Calif.	2
8	Asst. Naval Attache for Research, Office of Naval Research, American Embassy, London, England, Navy 100, F.P.O. New York, N.Y.	2
9	Director, Naval Research Laboratory, Office of Naval Research, Washington 25, D.C. Attn: Librarian	9
10	Bureau of Aeronautics, Dept. of the Navy, Washington 25, D.C., Attn: Aero and Hydro Branch (Code AD3)	2
11	Bureau of Ordnance, Dept. of the Navy, Washington 25, D.C., Attn: Code Re9 Code Re6 Code Re3	1 1 1
12	Commander, U.S. Naval Ordnance Laboratory, U.S. Navy Bureau of Ordnance, White Oak, Silver Spring 19, Maryland	2
13	Underwater Ordnance Dept., Naval Ordnance Test Station, 3202 E. Foothill Blvd., Pasadena, Calif. Attn: Pasadena Annex Library (Code P 5507)	3
14	Chief, Bureau of Ships, Dept. of the Navy, Washington 25, D.C. Attn: Technical Library (Code 312) for additional distribution to:	10

Distribution List (continued)

Item	Address	No. Copies
	(Bureau of Ships distribution) Research and Development (Code 300) Ship Design (Code 410) Preliminary Design (Code 420) Hull Design (Code 440) Hull Scientific (Code 442) Propeller Design (Code 554)	
15	Mr. R. H. Kent, Ballistic Research Laboratories, Dept. of the Army, Aberdeen Proving Ground, Maryland	1
16	Director of Research, National Advisory Committee for Aeronautics, 1512 H Street, N.W., Washington 25, D.C.	1
17	Director, Langley Aeronautical Lab., National Advisory Committee for Aeronautics, Langley Field, Virginia	1
18	Commander, Naval Ordnance Test Station, Inyokern, China Lake, Calif., Attn: Library (Code 5507)	1
19	Dr. K.S.M. Davidson, Experimental Towing Tank, Stevens Institute of Technology, Hoboken, N. J.	1
20	Dr. J.H. McMillen, National Science Foundation, 1520 H Street, N.W., Washington 25, D.C.	1
21	Dr. A. Miller, Bureau of Ordnance (Code Re3d) Navy Dept. Washington 25, D.C.	1
22	Dr. H. Rouse, Iowa Institute of Hydraulic Research, State University of Iowa, Iowa City, Iowa	1
23	Dr. R.G. Folsom, Director, Engineering Research Institute, University of Michigan, East Engineering Bldg. Ann Arbor, Michigan	1
24	Dr. V.L. Streeter, Engineering Dept., University of Michigan, Ann Arbor, Michigan	1
25	Dr. G.F. Wislicenus, Pennsylvania State University, Ordnance Research Laboratory, University Park, Pa.	1
26	Dr. A.T. Ippen, Dept. of Civil and Sanitary Engineering, Massachusetts Institute of Technology, Cambridge 39, Mass.	1
27	Dr. L.G. Straub, St. Anthony Falls Hydraulic Laboratory, University of Minnesota, Minneapolis 14, Minn.	1
28	Prof. K.E. Schoenherr, University of Notre Dame, College of Engineering, Notre Dame, Indiana	1
29	Director, Ordnance Research Laboratory, Pennsylvania State University, University Park, Pa.	1

Distribution List (continued)

Item	Address	No. Copies
30	Society of Naval Architects and Marine Engineers 74 Trinity Place, New York 6, N.Y.	1
31	Prof. J.K. Vennard, Stanford University, Dept. of Civil Engineering, Stanford, California	1
32	Prof. J.L. Hooper, Worcester Polytechnic Institute, Alden Hydraulic Laboratory, Worcester 6, Mass.	1
33	Prof. J.M. Robertson, Dept. of Theoretical and Applied Mechanics, University of Illinois, Urbana, Ill.	1
34	Dr. A.B. Kinzel, President, Union Carbide and Carbon Research Lab., Inc., 30 E. 42nd St., New York, N.Y.	1
35	Goodyear Aircraft Corp., Akron 15, Ohio, Attn: Security Officer	1
36	Prof. H.R. Henry, Hydraulics Laboratory, Michigan State College, East Lansing, Michigan	1
37	British Joint Services Mission, Navy Staff, Via: David Taylor Model Basin, Code 580, Navy Department, Washington 7, D.C.	9
38	Commander, Submarine Development Group TWO, Box 70, U.S. Naval Submarine Base, New London, Conn.	1
39	Commanding Officer and Director, U.S. Navy Engineering Experiment Station, Annapolis, Maryland	1
40	Library of Congress, Washington 25, D.C., Attn: ASTIA	1
41	Dr. P. R. Garabedian, Stanford University, Applied Mathematics and Statistics Laboratory, Stanford, California	1
42	Armed Services Technical Information Agency, Knott Building, Dayton, Ohio	5
43	Mr. J.G. Baker, Baker Manufacturing Company, Evansville, Wisconsin	1
44	Mr. T.M. Buerman, Gibbs and Cox, Inc., 21 West St., New York 6, New York	1
45	Dynamic Developments, Inc., St. Mark's Lane, Islip, Long Island, New York, Attn: Mr. W.P. Carl, Jr.	1
46	Hydrodynamics Research Laboratory, Consolidated-Vultee Aircraft Corporation, San Diego 12, California	1

Distribution List (continued)

Item	Address	No. Copies
47	Mr. R.K. Johnston, Miami Shipbuilding Corporation, 615 S.W. Second Avenue, Miami 36, Florida	1
48	Mr. J.D. Pierson, The Glenn L. Martin Company, Baltimore 3, Maryland	1
49	Mr. W.R. Ryan, Edo Corporation, College Point 56, Long Island, New York	1
50	Dr. Robert C. Seamans, Radio Corporation of America, Waltham, Massachusetts	1
51	Dr. A.G. Strandhagen, Department of Engineering Mechanics, University of Notre Dame, Notre Dame, Ind.	1
52	Dr. H.W.E. Lerbs, Hamburgische Schiffbau-Versuchsanstalt Hamburg 33, Bramfelderstrasse 164	1
53	Commander, Air Research and Development Command, P.O. Box 1395, Baltimore, Maryland. Attn: RDTDED	1
54	Avco Manufacturing Corp., Advanced Development Div., 2385 Revere Beach Parkway, Everett 49, Mass. Atten: Technical Librarian	1
55	Dr. L. Landweber, Iowa Inst. of Hydraulic Research, State University of Iowa, Iowa City, Ia.	1